5-31-2016

Prediction of the Frictional Characteristics of Halogen-Free Ionic Liquids in Elastohydrodynamic Point Contacts.

Karthik Janardhanan
kj7715@rit.edu

ROCHESTER INSTITUTE OF TECHNOLOGY

Prediction of the Frictional Characteristics of Halogen-Free Ionic Liquids in Elastohydrodynamic Point Contacts.

Submitted by,

Karthik Janardhanan

A Thesis Submitted in Partial Fulfillment of the Requirements for Master of Science
In Mechanical Engineering

Department of Mechanical Engineering

Kate Gleason College of Engineering

Approved by:

Dr. Patricia Iglesias	**----------**
Department of Mechanical Engineering	**(Advisor)**
Dr. Rui Liu	**----------**
Department of Mechanical Engineering	**(Committee Member)**
Dr. Stephen Boedo	**----------**
Department of Mechanical Engineering	**(Committee Member)**
Dr. Agamemnon Crassidis	**----------**
Department of Mechanical Engineering	**(Department Representative)**

Rochester Institute of Technology

Rochester, New York

5/31/2016

ABSTRACT

Ionic Liquids have emerged as effective lubricants and additives to lubricants, in the last decade. Halogen-free ionic liquids have recently started to be considered as more environmentally stable than their halogenated counterparts, which tend to form highly toxic and corrosive acids when exposed to moisture. Most of the studies using ionic liquids as lubricants or additives of lubricants have been done experimentally. Due to the complex nature of the lubrication mechanism of these ordered fluids, the development of a theoretical model that predicts the ionic liquid lubrication ability is currently incomplete. In this study, a suitable and existing friction model to describe lubricating ability of ionic liquids in the elastohydrodynamic lubrication regime is identified and compared to experimental results.

Two phosphonium-based, halogen-free ionic liquids are studied as neat lubricants and as additives to a Polyalphaolefin base oil in steel-steel contacts using a ball-on-flat reciprocating tribometer. Experimental conditions (speed, load and roughness) are selected to ensure that operations are carried out in the elastohydrodynamic regime. Wear volume was also calculated for all tests. A good agreement was found between the model and the experimental results when [THTDP][Phos] was used as an additive to the base oil, but some divergence was noticed when [THTDP][DCN] was added, particularly at the highest speed studied. A significant decrease in the steel disks wear volume is observed when 2.5 wt. % of the two ionic liquids were added to the base lubricant.

ACKNOWLEDGEMENTS

I would like to thank everyone who ensured that my research was a success through their constant support and guidance. First and foremost, I would like to thank my advisor Dr. Patricia Iglesias for giving me the opportunity to work with her. Her guidance and reassurance kept me going when times were hard and her enthusiasm for her work is something I will strive to achieve. I am also grateful for her unwavering trust in me and my work.

I would like to thank my committee members Dr. Agamemnon Crassidis, Dr. Rui Liu, and especially Dr. Stephen Boedo for his valuable advice. I would also like to thank Mr. Rob Kraynik for his assistance with sample preparation.

I would like to thank my fellow graduate students, Edward Cigno and Paarth Mehta for their help and all the good times in the lab.

Karthik Janardhanan.

CONTENTS

LIST OF FIGURES

LIST OF TABLES

NOMENCLATURE

a	=	cylinder diameter (m)
α	=	Barus' pressure-viscosity coefficient (GPa^{-1})
η	=	viscosity (cP)
p	=	ressure (MPa)
Z	=	Roelands pressure-viscosity index
h	=	film thickness (m)
U	=	speed (m/s)
E^*	=	Youngs reduced modulus (GPa)
R	=	effective radius of curvature (m)
λ	=	film parameter
σ	=	surface roughness (μm)
τ	=	shear stress (N/m^2)
ζ	=	limiting shear stress parameter
μ	=	coefficient of friction
G	=	Shear modulus(MPa)

SUBSCRIPTS

0	=	atmospheric value
r	=	Roelands constants
iv	=	isoviscous

1. INTRODUCTION

Friction has always been of interest to man from the very beginning. Whether it was to overcome friction or to use it beneficially, it has always been an important factor of consideration in engineering problems. In the transportation industry, overcoming friction is one of the main focus areas. In passenger cars for example, almost one third of the total energy is used to overcome friction in the tires, brakes, transmission and the engine as shown in Figure 1 [1].

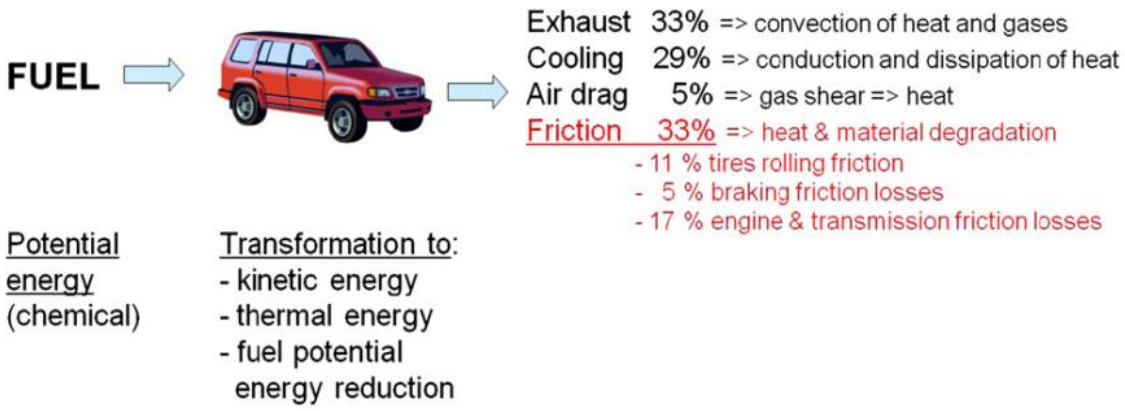

Figure 1: Loss of energy in passenger cars [1].

It is estimated that between 1 and 1.55% of a country's Gross Domestic Product (GDP) can be saved if friction and wear losses in mechanical parts were reduced. It is also estimated that approximately 11% of the total energy consumed in the U.S annually in the areas of transportation, turbomachinery, power generation, and industrial processes can be saved through new developments in lubrication and tribology [2].

Friction in machinery may be reduced using the following means:

- Low friction coatings
- Surface Topography and Texturing
- Lubricants
- Altering geometry of contacting surfaces

In the present study we will be concentrating on the effect of lubricants in friction reduction. Ionic Liquids (ILs) have recently been widely discussed in the context of tribology since 2001 [3]. ILs

are defined as salts which are liquids at temperatures below 100^0C. They consist of ion pairs which contain bulky, asymmetric cations and anions. The melting point and viscosity of these liquids are strongly dependent on their molecular structures, the length of alkyl chains and the type of cation and anion used. This provides for a large amount of variability and hence properties can be tailored to suit different complex situations [4]. The most important properties that allow ILs to be used in lubrication are: negligible volatility, non-flammability, high thermal stability, low melting point, and conductivity [4]. ILs also have a higher Viscosity Index when compared to commercial oils and hence there is a small variation in viscosity with temperature [5].

Another reason behind choosing ILs as our lubricant is the fact that they can be green substances when they are free of halogens [6]. This is the major advantage that these liquids hold over all the various commercially available lubricants.

The main aim of this study will be to identify a suitable, existing model which can effectively describe the lubrication mechanism of ILs, as neat lubricants (100% by weight) and as additives to lubricants. In this work we will focus on the interactions that take place in the Elastohydrodynamic lubrication regime and friction models used in this regime will be used to compare experimental findings so as to narrow down on an acceptable lubrication mechanism model.

2. THE RESEARCH QUESTION

Can an existing friction model be applied to successfully predict the behavior of ILs as lubricants? If so, under what specific conditions?

ILs have been proven to be very good lubricants by the means of experiments [4,7–10], however a friction model which can successfully describe these interactions is yet to be determined. The aim of this work is to identify such a model, if it exists, and to provide guidelines in the establishment of such a model in the event that an existing model is not suitable.

3. LITERATURE REVIEW

3.1 Friction in Elastohydrodynamic Lubrication

Elastohydrodynamic Lubrication (also referred to as EHL or EHD) is a form of hydrodynamic lubrication wherein the existence of a fluid film between two sliding contacts of high elastic modulus is explained by the elastic deformation of the surfaces under very high pressures and also by the increase in the viscosity of the fluid with pressure [11,12]. The first comprehensive numerical solution to the elastohydrodynamic problem was obtained by Dowson and Higginson [13], and the general formula obtained by them in 1959 is still in use today.

When dealing with the variation of viscosity with pressure, one of the simplest relations is the Barus' equation

$$\eta_p = \eta_0 e^{\alpha p} \tag{1}$$

where α is the pressure viscosity coefficient of the lubricant [14]. Another popular pressure-viscosity relation was proposed by Roelands [15]:

$$\eta = \eta_0 \, e^{\{ln\left(\frac{\eta_0}{\eta_R}\right)\left[\left(1+\frac{p}{p_R}\right)Z-1\right]\}} \tag{2}$$

where, η_r and p_R are reference viscosity and pressure and are given by $\eta_R = 6.315 \times 10^{-5}$ Pa s and $p_R = 1.98\times10^8$ Pa. The negative value of p_r is a fictitious negative pressure which gives a value of viscosity equal to η_r. Z is a constant and is known as the pressure-viscosity index.

Various rheological models for evaluating the friction coefficient in the EHD regime exist. The general approach used is to determine the surface shear stress using these models. The shear stress is then integrated over the contact area to determine the shear traction force and thereby the coefficient of friction is determined [16]. Otero et al. [17] have used two models to describe the frictional characteristics of Polyalphaolefins used in point contacts. They have then used a Multi Traction Machine (MTM) to obtain the friction coefficient experimentally. An approach similar to what they have conducted will be used in this study with different lubricants: a Polyalphaolefin with an IL as an additive, and an IL as a neat lubricant will be used.

Based on the load, elasticity and sliding speed planned in this thesis, the regime of lubrication can be set and in this case the elastohydrodynamic regime will be used. Using the chart of Hamrock and Dowson, Otero et al. selected the following correlation to calculate the central film thickness:

$$h_c = 1.39\left(\frac{\eta_0 U}{2E^* R}\right)^{0.67}(\alpha E^*)^{0.53}\left(\frac{E^* R^2}{W}\right)^{0.067} \quad (3)$$

where η_0 is the viscosity at atmospheric pressure, W is the load, α is the pressure viscosity coefficient, U is the average velocity between surfaces, E^* is the Young's reduced modulus and R the reduced radius of curvature.

It should be noted that Eq (3) is valid for unidirectional motion only. In the present study, a reciprocating friction tester will be used, and for the large stroke length to be used with this tester, it has been shown that that Eq (3) is valid for reciprocating motion as well at the maximum sliding velocity [18].

Once the film thickness is known, a surface roughness parameter can be calculated. This is used to determine if a smooth surface elastohydrodynamic regime can be considered. Given the surface roughness of the two mating surfaces (σ1, σ2) we have the film parameter $\lambda = \frac{h_c}{\sqrt{{\sigma_1}^2+{\sigma_2}^2}}$. If the film parameter is greater than 3, then it can be considered to be in the fully lubricated elastohydrodynamic regime.

3.1.1 Limiting Shear Stress model:

In a Newtonian fluid with a Barus Pressure-viscosity model, the shear stress is given by

$$\tau = \frac{\eta_0 e^{\alpha p}\Delta U}{h_c} \quad (4)$$

where p is the pressure and ΔU is the sliding velocity between the surfaces. However, studies have shown that there is a limiting shear stress at which the above formulation is no longer valid. Hence, an approach is chosen wherein the Newtonian model is considered until this limiting value is reached, and then the boundary value is considered. The boundary value is given by

$$\tau = \tau_L = \tau_0 + \zeta p \quad (5)$$

The limiting shear stress at atmospheric pressure (τ_0) and the limiting shear stress-pressure parameter (ζ) are constants specific to each lubricant.

The traction force is then obtained by integrating the shear stress over the area and from the traction force, the coefficient of friction is determined. The expression for the traction coefficient is given as

$$\mu = \frac{3\eta_0 \Delta U}{h_c}.(e^{m\alpha p_0}(m\alpha p_0 - 1) + 1)\frac{1}{\alpha^2 {p_0}^3} + \zeta(1 - m^3) \tag{6}$$

where, p_0 is the maximum film pressure(or Hertz pressure) and m is a parameter which measures the relation between the transition radius *b* and the contact radius *a* [19]. They are calculated using the following

$$p_0 = \frac{3W}{2\pi a^2};\ a = \sqrt[3]{\frac{3WR}{4E^*}};\ m = \sqrt{1 - (\frac{b}{a})^2};\ b = a\sqrt{1 - (\frac{p^*}{p_0})^2}$$

This model does not consider a transition zone between Newtonian and Non-Newtonian behavior. Because of this, an overestimation of the shear stress occurs, and hence the results are fairly inaccurate.

3.1.2 Carreau's Model

Carreau provided a generalized viscosity formula of the form[17]

$$\frac{\eta}{\eta_0 e^{\alpha p}} = \left[1 + \left(\frac{\frac{\eta_0 e^{\alpha p} \Delta U}{h_c}}{G}\right)^2\right]^{\frac{n-1}{2}} \tag{7}$$

Exponent n and shear modulus G are lubricant specific properties which are obtained by curve fits to data. The calculating process is similar to that carried out in the Limiting Shear Stress model. The final expression for the friction coefficient is given as:

$$\mu = 3\left(\frac{\eta_0 \Delta U}{h_c}\right)^n G^{1-n}.(e^{n\alpha p_0}[n\alpha p_0 - 1] + 1)\frac{1}{(n\alpha)^2 p_0^3} \tag{8}$$

The results obtained by Otero et al. are depicted in Figures 2 and 3.

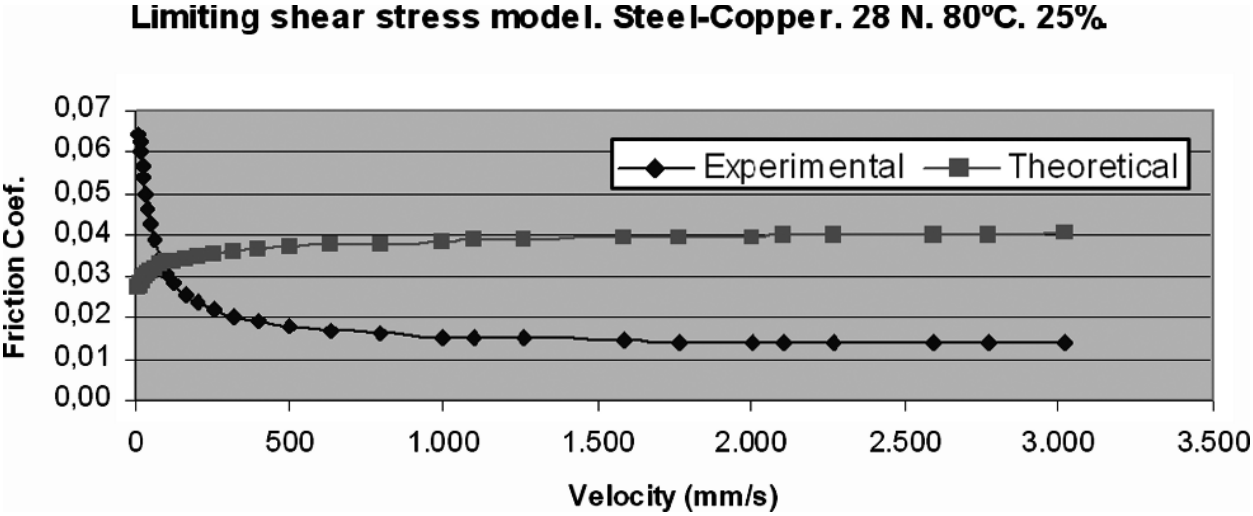

Figure 2: Results using the Limiting Shear Stress model [17].

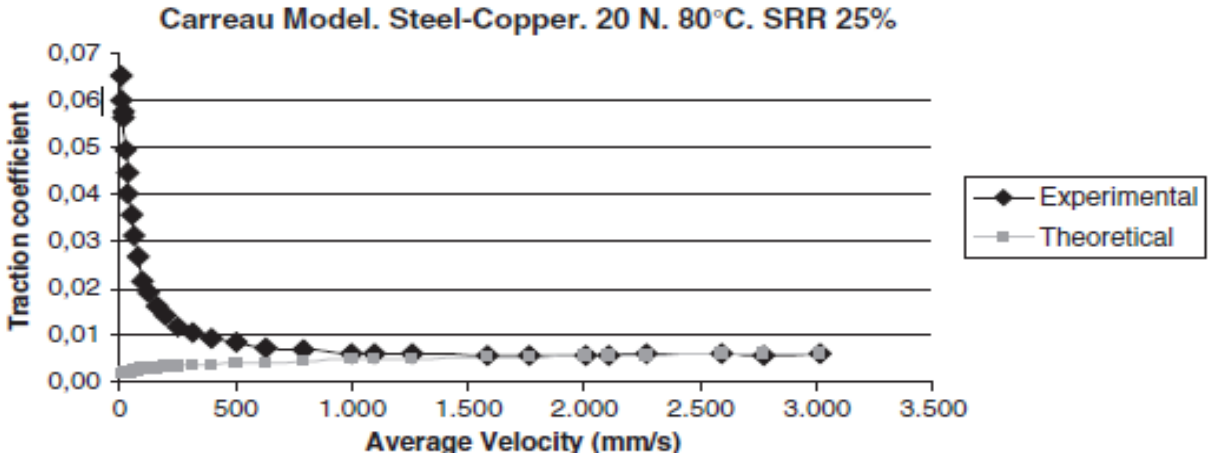

Figure 3: Results using Carreau's model [17].

From the figures, we see that Carreau's model agrees much better than the Limiting Shear Stress Model as a transition zone has been considered between the Newtonian and Non-Newtonian behavior of the fluid.

3.2 Ionic Liquids in Tribology

As mentioned before, ILs are salts which have a melting point lower than a 100^0C. ILs have certain properties which make them very good lubricants. These are high thermal stability, low melting point, non-flammability, conductivity and negligible volatility. Another characteristic that

distinguishes it from other synthetic lubricants is its high polarity. The high polarity allows these liquids to form an adsorption film and a tribochemical surface reaction which increases their anti-wear capabilities [4,9,20].

ILs can be used as base oils and as additives to base oils. The effects of Alkyl Imidazolium based ILs, both as a neat lubricant, and as an additive to a mineral oil in steel-aluminum contacts were recently studied. They found that overall, a very low friction coefficient was obtained when used as a neat lubricant but a further reduction (69-75%) in friction coefficient was obtained when 1 wt. % of an ionic liquid was used. (At 25 $^{\circ}$C). This was due to the lack of tribocorrosion processes at such concentrations [7].

The same authors also used ILs in steel-titanium contacts at 0 and 100 $^{\circ}$C using imidazolium and ammonium salts and have observed a 60% reduction in friction when compared to mineral oils at room temperatures [8].

Most of today's machinery is comprised of steel and hence a large number of surface contacts are steel-steel contacts. These contacts have been extensively studied with ILs as lubricants, and in particular, imidazolium salts with tetrafluorborate and hexafluorophosphate [3,7,8,21,22]. However these choices were mainly chosen as they have properties similar to conventional synthetic lubricants, and also because the imadozole cation is a versatile building block around which molecules which have appropriate physical and chemical properties [20]. But, it has been found that short chain imidazolium and ammonium are less hydrophobic and can absorb moisture which is undesirable.

Halogen Free Ionic liquids:

Tribology can also be considered "Green" when the fluid lubricant used is not hazardous to the environment. The aim of this research will be to determine if ILs which are halogen free, and thereby 'green' can be used to provide efficient lubrication. Most of the commercially available lubricants today have additives which are potentially harmful to the environment. Green ionic lubricants are expected to stable chemically and thermally, non-volatile liquids, environmentally inert and in some cases, biodegradable, while at the same time, reducing friction and wear efficiently. As mentioned above, most of the ILs used today contain harmful elements such as [BF4]-, [PF6]-, [SO3CF3]-, [NTf2] - etc. These are potentially very harmful as when [BF4]-and

[PF6]- are hydrolyzed, they form HF which is highly corrosive [23]. Thus we find the need to find highly stable, environmentally friendly "Green Ionic" liquids which are high performance lubricants which can replace commercially available lubricants.

Gusain et al. [24] used bis(salicylate)borate as an anion with imidazolium and ammonium salts and found that their performance was very good when used as an additive to a base oil (PEG 200). These ions have the added advantage that as they are sulphur, phosphorous and halogen free, they protect surfaces from tribo-corrosion and are also environmentally friendly

Minami et al. [25] studied the tribo-chemistry of phosphonium derived ILs and found that under similar loading conditions, the phosphonium salts performed better when compared to an imidazolium salt. It was also noted that phosphate and thiophosphate anions produced better results when compared to TFSA (trifluoromethylsulfonyl). It was also found that phosphonium phosphate, when used as an additive, produced a much lower wear volume when compared to BMIM-NTf2 [23]. Phosphonium based ILs will be used in the present study as they have been proven to be very effective lubricants in steel-steel contacts, and they have an added advantage of being halogen free.

3.3 Ionic Liquids as lubricants in Elasto-Hydrodynamic contacts.

Pensado et al. [22] obtained the universal pressure-viscosity coefficient for a group of imidazolium based ILs. The viscosity and density as a variation of pressure and temperature was obtained from already published values for these liquids [26–31]. The reciprocal asymptotic isoviscous pressure coefficient was calculated using Blok's isoviscous pressure relation

$$\alpha^* = \frac{1}{p_{iv(\infty)}} = \left[\int_0^\infty \frac{\eta(p=0)dp}{\eta(p)}\right]^{-1} \quad (9)$$

From which the universal pressure-viscosity coefficient was found using Bair's relation given by

$$\alpha_{film} = \frac{1-e^{-k}}{p_{iv}\left(\frac{k}{\alpha^*}\right)} \quad (10)$$

Where k=3 was empirically chosen for accuracy. Bair also found that that this value of α_{film} could be used to calculate film thickness in equation (3) [32].

The pressure viscosity coefficient obtained by Pensado for ILs is shown in Tables 1 and 2.

Table 1: α^* (GPa^{-1}) values obtained by Pensado [22]

T/K	$[C_4C_1im]BF_4$	$[C_4C_1im]PF_6$	$[C_4C_1im]Tf_2N$	$[C_6C_1im]PF_6$	$[C_6C_1im]Tf_2N$	$[C_8C_1im]BF_4$	$[C_8C_1im]PF_6$
283.15	11.5		12.4		10.3		
293.15	10.4		11.3		9.8		
298.15	9.9	13.2	10.7	13.7	9.5	11.1	13.3
303.15	9.4	12.6	10.2	13.1	9.3	10.7	12.8
313.15	8.6	11.4	9.4	12.0	8.9	9.8	11.8
323.15	7.8	10.5	8.6	11.1	8.6	9.0	11.1
333.15	7.2	9.6	7.9	10.2	8.3	8.3	10.3
343.15	6.6	8.8	7.3	9.5	8.1	7.7	9.6
353.15	6.1	8.1	6.8	8.8	7.7	7.2	9.0

Table 2: α_{film} (GPa^{-1}) values obtained by Pensado [22]

T/K	$[C_4C_1im]BF_4$	$[C_4C_1im]PF_6$	$[C_4C_1im]Tf_2N$	$[C_6C_1im]PF_6$	$[C_6C_1im]Tf_2N$	$[C_8C_1im]BF_4$	$[C_8C_1im]PF_6$
283.15	11.7		12.8		10.4		
293.15	10.6		11.6		9.8		
298.15	10.1	13.5	11.1	14.1	9.5	11.7	13.9
303.15	9.7	12.9	10.6	13.5	9.2	11.2	13.3
313.15	8.8	11.8	9.8	12.4	8.8	10.3	12.4
323.15	8.2	10.9	9.1	11.6	8.5	9.6	11.7
333.15	7.5	10.0	8.4	10.7	8.1	8.8	10.9
343.15	6.9	9.3	7.8	9.9	7.8	8.2	10.2
353.15	6.3	8.6	7.1	9.3	7.5	7.7	9.6

Pensado et al. states that these obtained values are lower than that of most conventional oils used in aerospace and gear lubrication applications. However, this does not mean that these liquids can not be used in EHL contacts and it actually favors their use as a lower value of the pressure viscosity coefficient implies that there will be a reduction in friction energy as well as pressure spikes, which play an active role in wear and failure of gear elements and bearings.

An alternative method of determining a pressure-viscosity relation is presented. The Roelands pressure-viscosity index can be approximated from the relation given by Roelands [15,33].

$$Z = [7.81(H_{40} - H_{100})]^{1.5} F_{40} \tag{11}$$

where,

$F_{40} = (0.885 - 0.864H_{40});\ H_{40} = \log(\log(\eta_{40}) + 1.200)\,; H_{100} = log(log(\eta_{100}\ ) + 1.200)$

The above correlation gives good estimates for synthetic hydrocarbons, polymers, diesters, and polyolesters and for hydrocarbon and ester-base oils with additives [33].

If we assume that at ambient pressure (p=0), the slopes of the Barus and Roelands equation are equal, then the Barus parameter can be obtained from the Roelands one using [34].

$$\alpha = \frac{zln\left(\frac{\eta_0}{\eta_r}\right)}{p_r} \tag{12}$$

Moes [35] shows that α^* can be related to α using the following approximation,

$$\alpha^* \approx \frac{\alpha}{1+\left((1-z)(\alpha p_r)\right)} \tag{13}$$

The validity of these relations was verified by comparing the results with published values of three commercial lubricants and three ILs. The results are shown in Table 3, in chapter 4.

4. OBJECTIVES

The objectives of the proposed work will be to:

- Perform tests to measure the friction coefficient using ILs as lubricants and additives to lubricants.
- The ILs will be added in concentrations of 0.5%, 1% and 2.5% by weight to the base oil.
- Measure the viscosity of the ILs and mixtures and calculate the pressure-viscosity coefficient for all lubricants
- Theoretically calculate the coefficient of friction using the identified rheological models and therefore either validate or invalidate the models with the experimental data, for their usage with the chosen ILs.
- Measure the wear width and calculate the wear volume of the test samples after a time interval of one hour.

5. WORK PERFORMED

5.1 Preliminary Work

Limited work relating to the rheological models has been done. The pressure-viscosity calculations suggested by equations (11-13) were validated using 6 lubricants, 3 of which were ILs, using the published values for the viscosity at 40 and 100^0C. The obtained results were compared with the values published by Pensado et al [22].

Table 3: Validation of Pressure-Viscosity Coefficient calculations. (Equations 11-13)

Lubricant	Published	Calculated	Absolute Error
Mineral Oil	20.73	20.692	0.038
PAO	13.401	14.796	1.395
PAG	11.041	8.3982	2.6428
[C4C1im]BF4	8.6	17.068	8.468
[C6C1im]PF6	12	19.8	7.8
[C4C1Im]Tf2N	9.8	13.75	3.95

From Table 3, the absolute error between published and calculated data is small for mineral oils and PAO. However, larger error is seen in the case of the three ILs. In the present study, ILs are going to be used as additives to a base lubricant which is a PAO. The concentrations of these ILs added are going to be in the range of 1-5% and, hence, the overall expected error in the estimation of the pressure-viscosity coefficient is low. Also, it is to be noted that the published values for the mineral oil, PAO and PAG depict the Barus pressure-viscosity coefficient while the one calculated in this work, is the isoviscous pressure viscosity coefficient which is found to be more accurate.

5.2 Experimental Details

5.2.1 Tribological Details

AISI 52100 steel flat disks (19 mm diameter, 243 hardness HV, Roughness Ra=0.1-0.4 μm) were tested in a ball-on-flat reciprocating tribometer (figure 4 and 5) against AISI 420C steel balls (1.5 mm spherical diameter, 690 hardness HV, Roughness Ra=0.05 μm). Tribological tests were carried out at room temperature and under a normal load of 5 N (2.75 GPa maximum Hertzian pressure), and three different speeds of 0.01 m/s, 0.02 m/s and 0.04 m/s. The speeds were achieved by varying the stroke length (2.5 mm,5 mm,10 mm) while using a constant frequency of 2Hz. The slide-roll ratio was kept constant during tests. The roughness was varied according to the speed to ensure that the film parameter (λ) was always between 3 and 10, thereby ensuring we were operating in the elastohydrodynamic regime. Table 4 shows the values of roughness used at different speeds and the calculated film parameter. As the film parameter is always between 3 and 10, we ensure that we are operating in the elastohydrodynamic regime.

Table 4: Roughness values at each speed.

Speed (m/s)	**Roughness (μm)**	**Film Parameter (λ)**
0.01	0.10	6.29
0.02	0.20	6.82
0.04	0.40	6.98

Friction coefficients were continuously recorded with sliding distance. Mean friction coefficients and wear volume were obtained after three tests under the same conditions. Volume loss (Vf) was determined by image analysis after 45 wear track width (Wt) measurements for each test, according to Eq. (14) [36]:

$$V_f = L_s\left[R_f^2 * \sin^{-1}\left(\frac{W_t}{2*R_f}\right) - \left(\frac{W_t}{2}\right)\left(\frac{R_f}{h_f}\right)\right] + \frac{\pi}{3}(3R_f - h_f) \quad (14)$$

Where L_s is stroke length, R_f is the radius of 440C steel ball and h_f is the wear depth given by Eq. (15)

$$h_f = R_f - \sqrt{R_f^2 - \frac{W_t^2}{4}} \quad (15)$$

5.2.2 Lubricants

The base lubricant for this study is a Polyalphaolefin (PAO), specifically, Synton PAO-40, a synthetic oil. Two ionic liquids are used as additives to the base lubricant. The ionic liquids used were obtained commercially from Sigma-Aldrich (USA). Their names, structure and IUPAC name are presented in Table 5.

Table 5: Names and structures of ILs used in this study.

Code	Structure		IUPAC name
	Cation	Anion	
[THTDP][DCN]	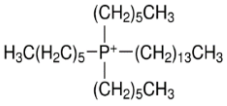	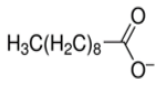	Trihexyltetradecylphosphonium decanoate
[THTDP][Phos]		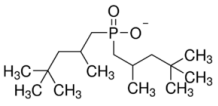	Trihexyltetradecylphosphonium bis(2,4,4)trimethylpentyl)phosphinate

5.2.3 Viscosity Measurements

The viscosities of all lubricants and mixtures were measured using a Brookfields DVII+ Viscometer with a Thermosel attachment. Measurements were made at temperatures of 40˚C and 100˚C.

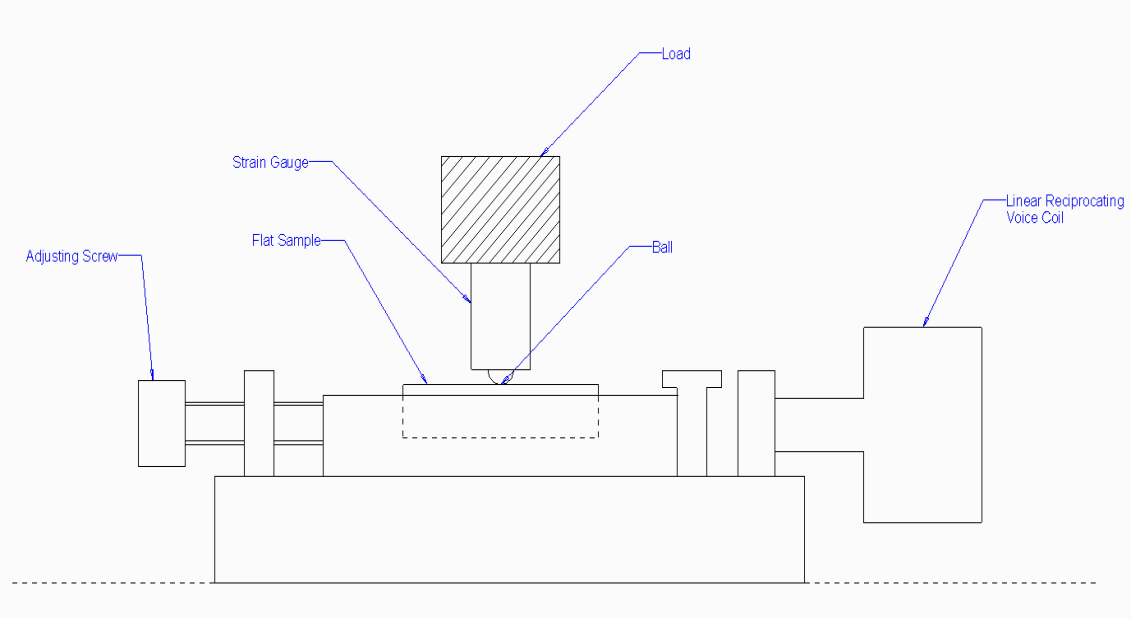

Figure 4: Schematic of ball-on-flat test configuration

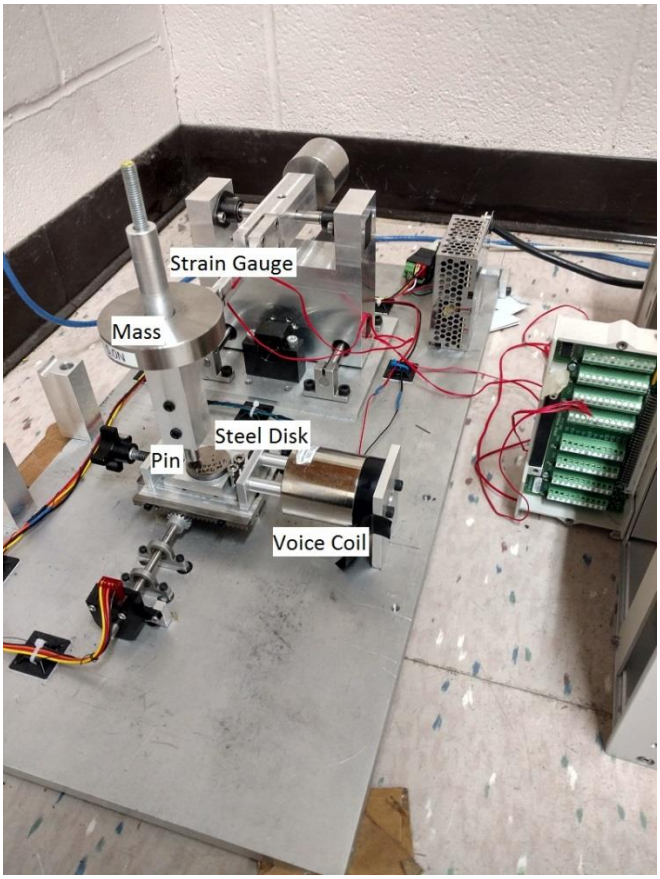

Figure 5: Reciprocating Tribometer

6. RESULTS

6.1 Viscosity and Pressure-Viscosity Coefficient Results

The viscosity values at 40°C and 100°C, and the calculated pressure-viscosity coefficient (α^*) for all lubricants used in this study are presented in Table 6. As seen in the table, the addition of the IL's to the base oil slightly increases the viscosity of the PAO. This increase is also noticed in the pressure-viscosity coefficient.

As seen in Table 6, the viscosity of [THTDP][DCN] at 40°C couldn't be obtained as it is a semi-solid at this temperature.

The [THTDP][Phos] also exhibits an interesting behavior due to the fact that its viscosity decreases as the speed, at which the viscosity is measured, is increased. Hence we conclude that this liquid exhibits what is known as shear thinning. Shear thinning is a phenomenon which occurs in certain fluids where the viscosity of the fluid decreases as the shear rate is increased. As the viscosity varies with shear rate, the [THTDP][Phos] can be classified as a non-Newtonian fluid. Figure 6 describes the variation of the viscosity of [THTDP][Phos] with speed at 40°C and 100°C.

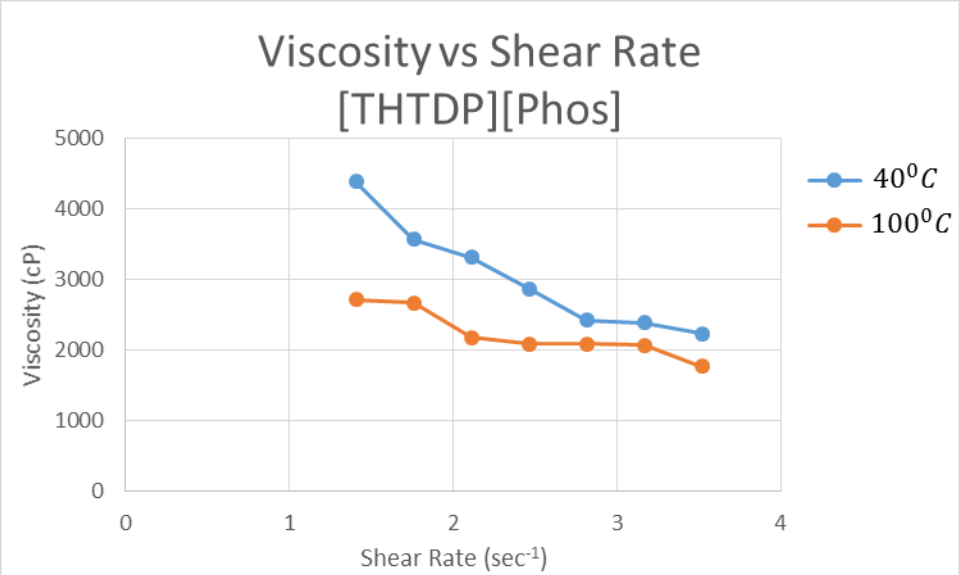

Figure 6: Viscosity of [THTDP][Phos] vs Shear Rate(sec^{-1})

In Table 6, the value of viscosity at a spindle speed of 0.6 RPM is listed as this speed corresponds to the speeds at which the tribometer was run. However, the obtained value of the pressure-viscosity coefficient appears to be incorrect when compared to the other lubricants.

A similar test was carried out with [THTDP][DCN] at 100°C to determine if the same behavior is noticed.

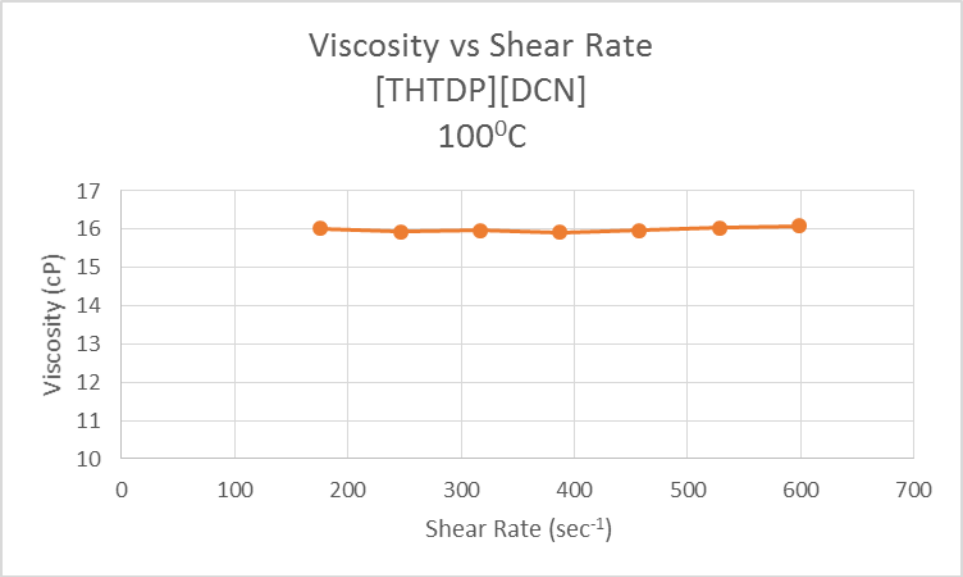

Figure 7: Viscosity of [THTDP][DCN] vs Shear Rate(sec^{-1})

Figure 7 shows that [THTDP][DCN] does not exhibit any shear thinning behavior and the viscosity remains constant as the rate of shear is increased. This can be classified as a Newtonian liquid.

Table 6: Viscosity and Pressure-Viscosity Coefficient of lubricants

Lubricant	Viscosity(cP)		Pressure Viscosity Coefficient $\alpha^{*}(GPa^{-1})$
	40^0C	100^0C	
PAO	325.00	32.00	16.38
PAO+0.5%[THTDP][Phos]	330.09	32.34	16.39
PAO+1%[THTDP][Phos]	330.35	32.18	16.47
PAO+2.5%[THTDP][Phos]	331.99	32.13	16.55
PAO+0.5%[THTDP][DCN]	339.00	32.70	16.51
PAO+1%[THTDP][DCN]	360	32	17.52
PAO+2.5%[THTDP][DCN]	343.30	30.85	17.56
[THTDP][Phos] (at 0.6 rpm)	3310	2180	0.12*
[THTDP][DCN]	Semi-Solid	17.3	-

6.2 Experimental Friction Results

The experimental results obtained from the ball on flat reciprocating tribometer are documented in this section. Continuous friction data was obtained from the tribometer and a moving average of this data was collected in order to show trends. Each test was performed thrice in order to obtain consistent results. Figures 8 and 9 show the plot of the friction coefficient vs time for each lubricant at 0.01 m/s. These plots depict the average friction coefficient obtained from the three tests conducted.

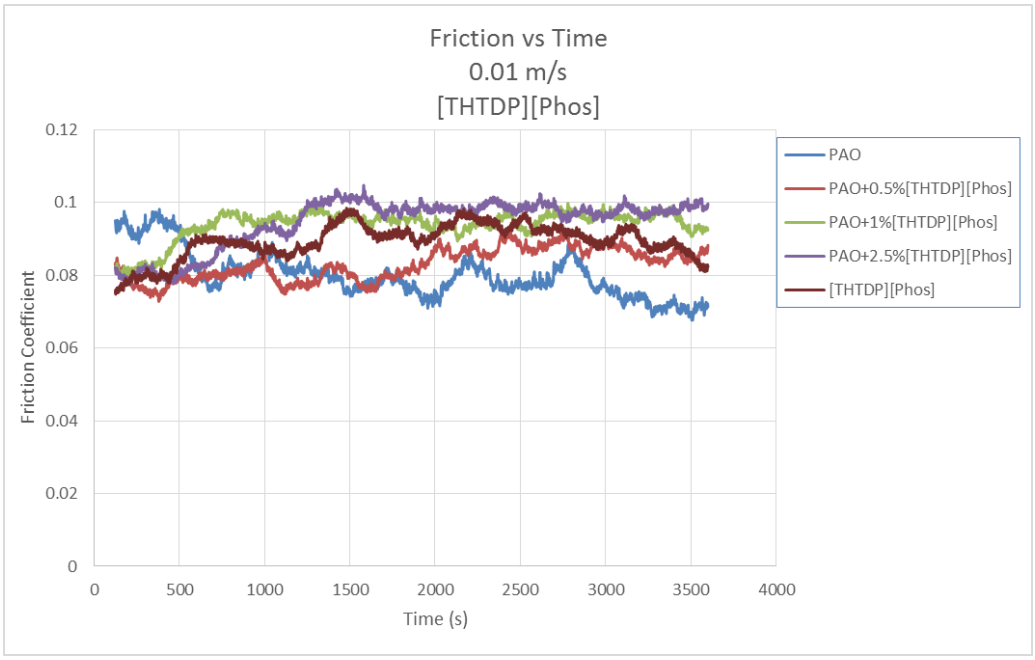

Figure 8: Mean friction coefficient vs time using [THTDP][Phos] as neat lubricant and as an additive to PAO at 0.01 m/s

From figure 8, there is no significant change in the coefficient of friction when [THTDP][Phos] is used as a neat lubricant or as an additive to PAO at this particular speed.

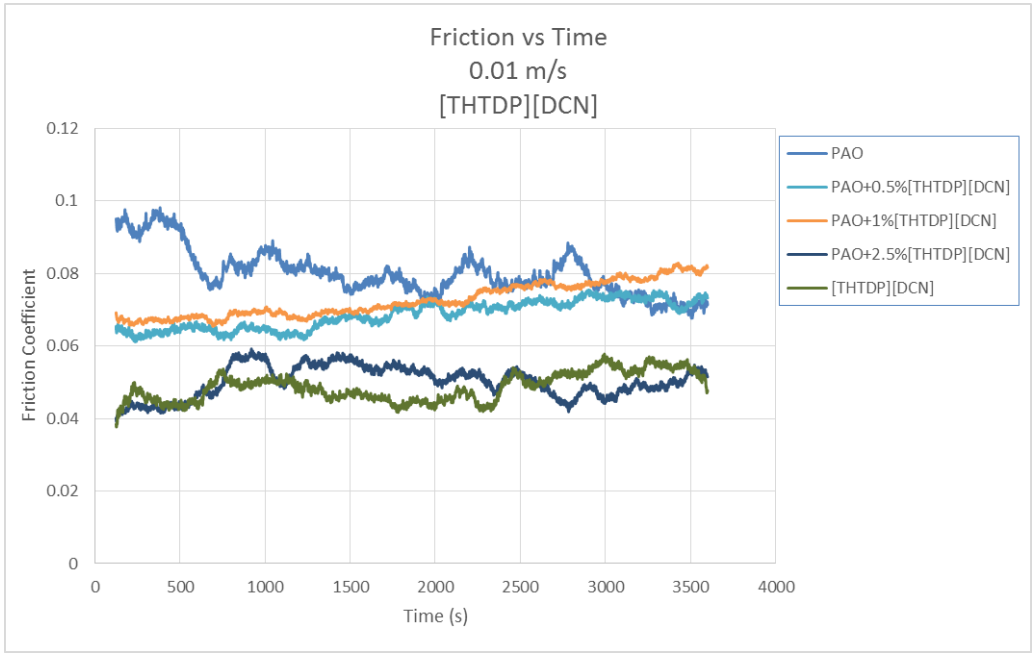

Figure 9: Mean friction coefficient vs time using [THTDP][DCN] as neat lubricant and as an additive to PAO at 0.01 m/s

Figure 9 shows the friction coefficients as a function of time of PAO, [THTDP][DCN] as neat lubricant and [THTDP][DCN] as additive in PAO. From the figure, an important reduction in friction can be seen in almost all cases, except at the end of the test where the PAO performs slightly better than when 0.5% and 1% of the IL are added. A large reduction in friction is observed when 2.5% and the neat IL is used. It should also be noted that a more constant friction coefficient over the entire test cycle is achieved when the IL is used. The mean (and standard deviation) friction coefficient obtained for each lubricant is summarized in Figure 10.

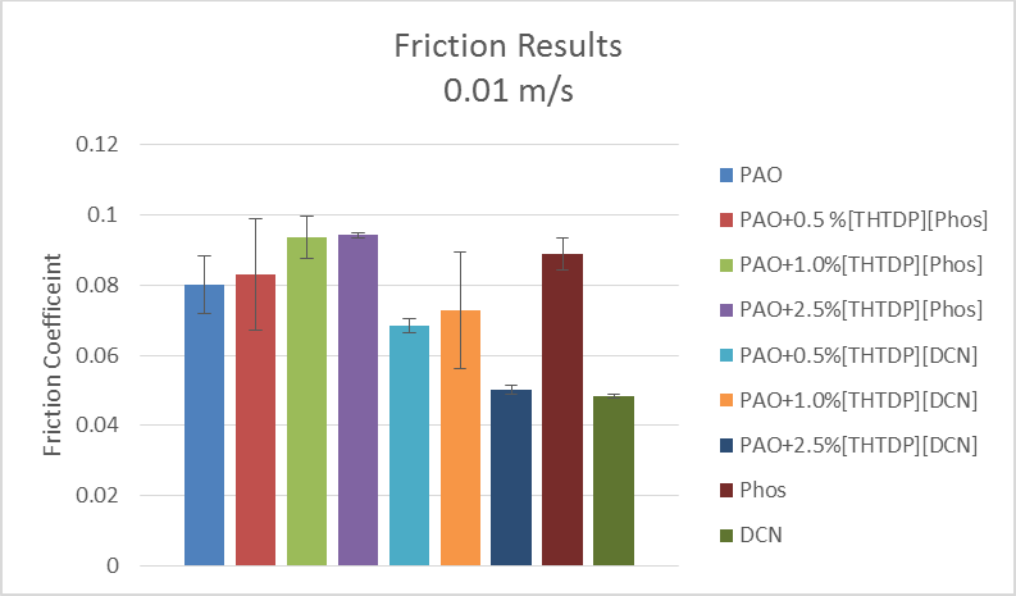

Figure 10: Summary of Friction results at 0.01 m/s

When the speed is increased to 0.02 m/s, the performance [THTDP][Phos] (Figure 11) is similar or better than that of the PAO except when 2.5% of the IL is added to the base oil. A drastic reduction is noticed when 0.5% and 1% of the IL is used as an additive. In comparison, [THTDP][DCN] (Figure 12) slightly affects the frictional properties of the base oil at this particular speed. A reduction in friction is observed when 1% and 2.5% of this IL is used as an additive to the PAO.

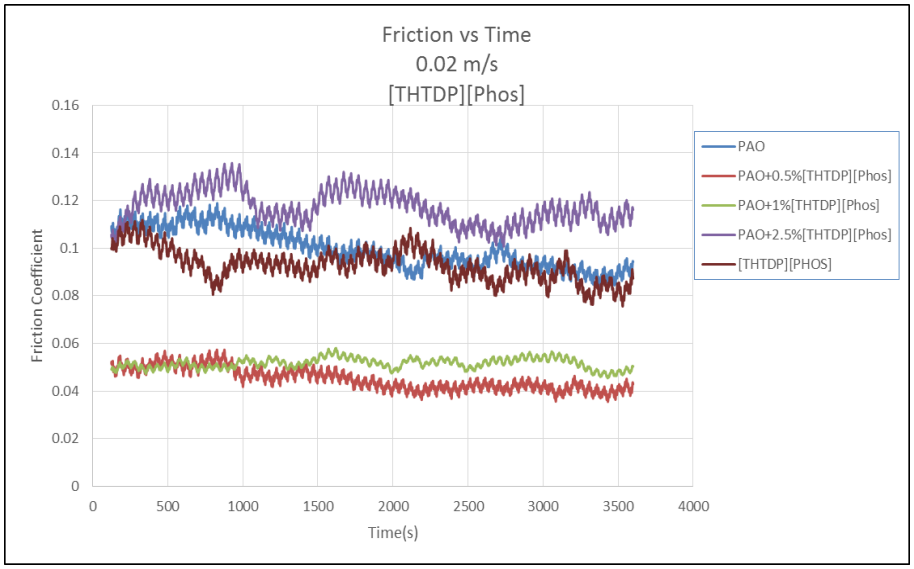

Figure 11: Mean friction coefficient vs time using [THTDP][Phos] as neat lubricant and as an additive to PAO at 0.02 m/s

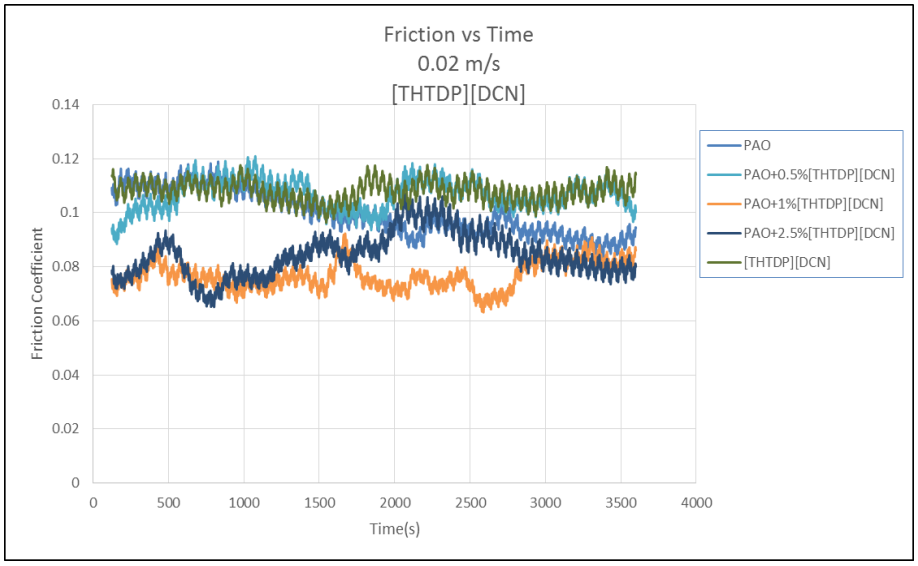

Figure 12: Mean friction coefficient vs time using [THTDP][DCN] as neat lubricant and as an additive to PAO at 0.02 m/s

The average friction values for each lubricant are summarized in Figure 13.

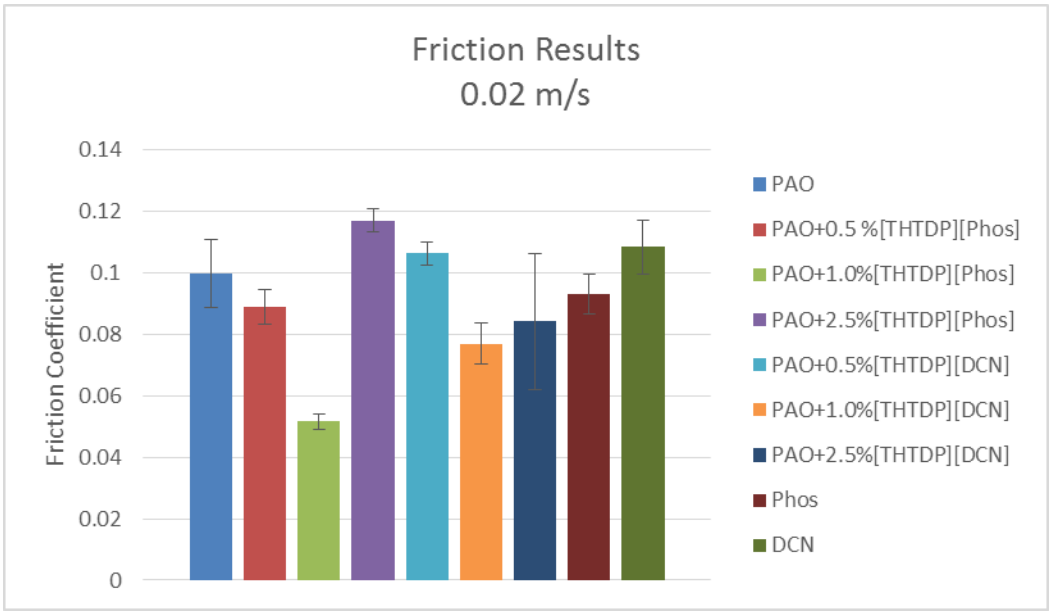

Figure 13: Summary of friction results at 0.02 m/s

Figures 14 and 15 show the results obtained at a speed of 0.04 m/s. As can be seen, the only significant reduction in friction is obtained when [THTDP][DCN] is used as a neat lubricant.

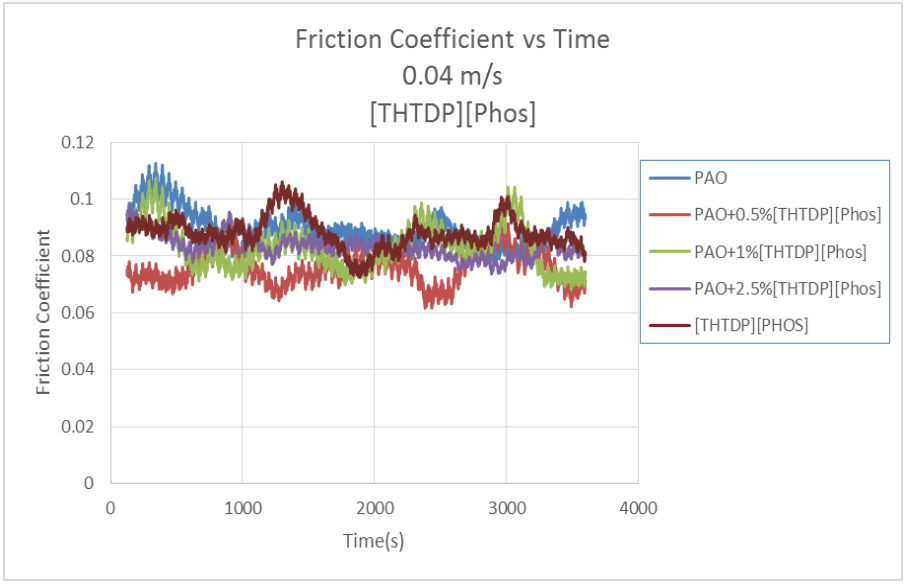

Figure 14: Mean friction coefficient vs time using [THTDP][Phos] as neat lubricant and as an additive to PAO at 0.04 m/s

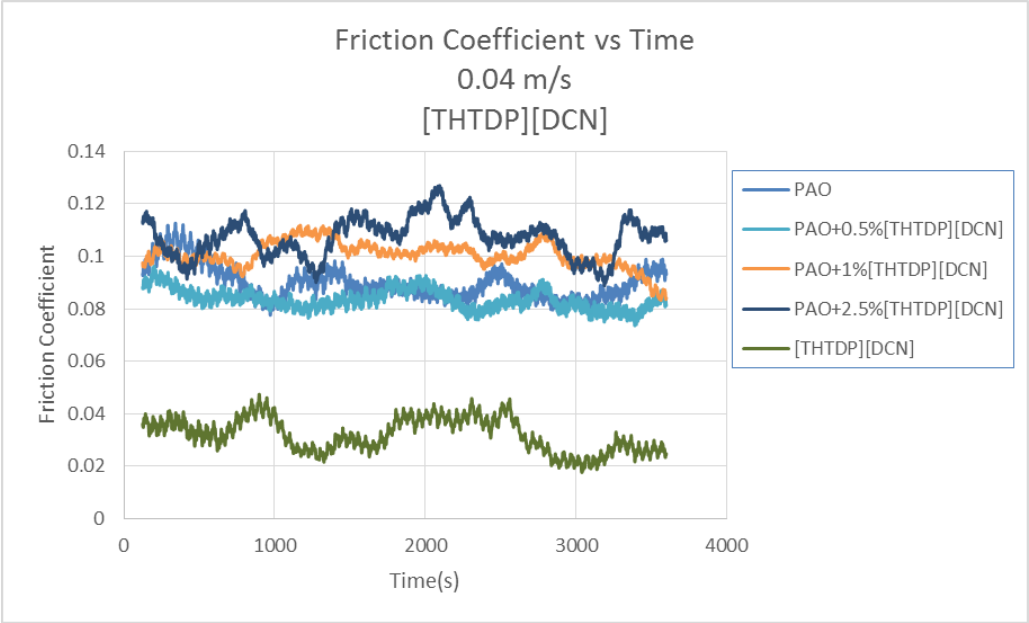

Figure 15: Mean friction coefficient vs time using [THTDP][Phos] as neat lubricant and as an additive to PAO at 0.04 m/s

Figure 16 shows the mean friction values of each lubricant at 0.04 m/s.

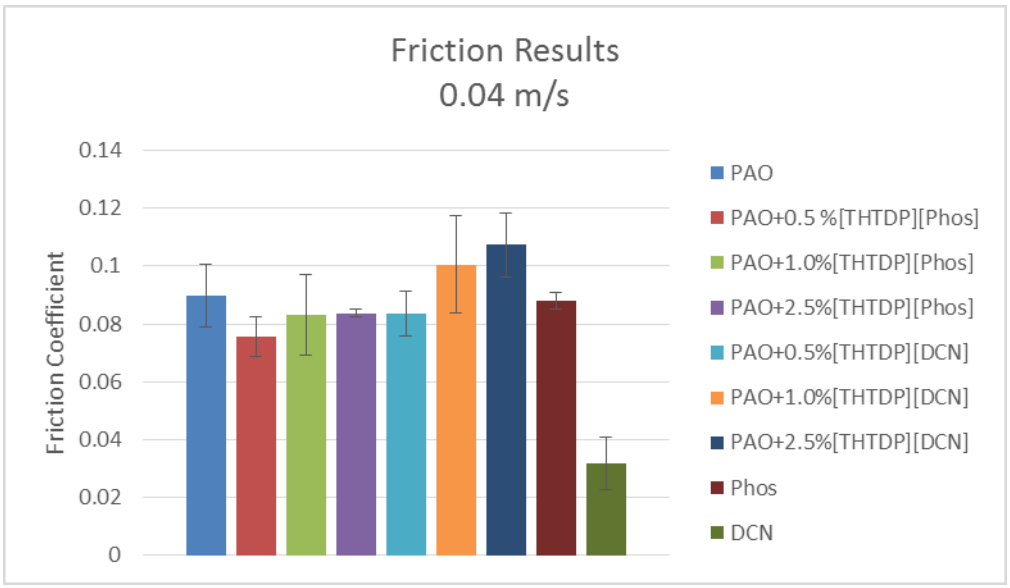

Figure 16: Summary of friction results at 0.04 m/s

Figures 17 and 18 show the variation of friction coefficient with speed. From figure 17, addition of [THTDP][Phos] to the base oil causes a decrease in the friction coefficient, when compared to

the neat PAO, at lower concentrations. A higher friction coefficient is observed at lower speeds when 2.5% wt. is added to the base oil, however at higher speeds a lower friction coefficient is observed. Also it is noted that the lowest friction coefficient is observed at the medium speed when 1% wt. is added.

In the case of the [THTDP][DCN] (Figure 18), a reduction in friction is observed at lower speeds when higher concentrations are added to the PAO. The greatest reduction in friction is observed when [THTDP][DCN] is used as a neat lubricant at higher speeds. It must be noted that as this IL is semi-solid at room temperature, it was initially heated till its melting point and then used as a liquid lubricant.

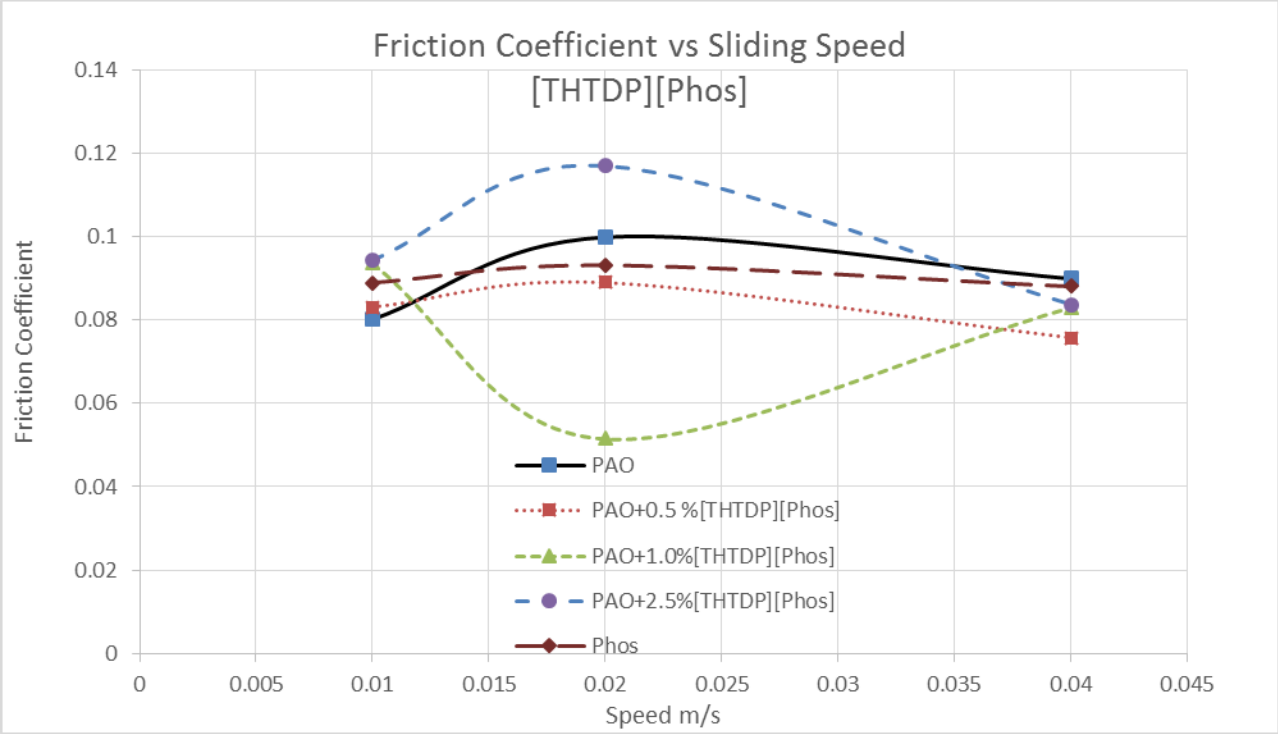

Figure 17: Friction coefficient vs Sliding Speed when [THTDP][Phos] is used as a neat lubricant and as an additive to PAO

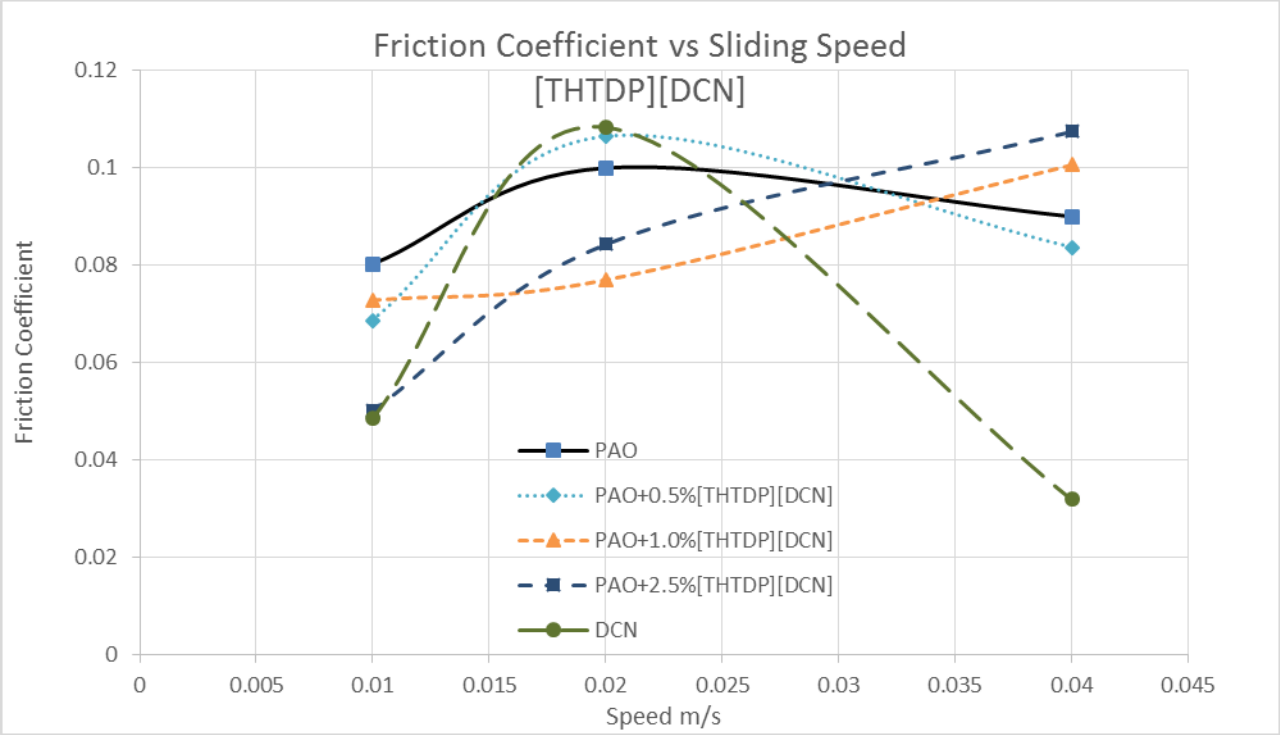

Figure 18: Friction coefficient vs Sliding Speed when [THTDP][DCN] is used as a neat lubricant and as an additive to PAO

6.3 Comparison of Experimental Friction Results with Carreau's Model

Figures 19-21 compare the experimental results with those obtained from Carreau's model. The parameters n and G which appear in Carreau's model were obtained by a least squares based parameter estimation. The obtained values are consistent with those published for polyalphaolefins [37]. These values are documented in Table 7.

Table 7: Values of exponent n and Shear Modulus G obtained from data

Lubricant	n	Shear Modulus G *10^6 Pa
PAO	0.1235	4.2859
PAO+0.5%[THTDP][Phos]	0.1242	4.3415
PAO+1%[THTDP][Phos]	0.1275	4.2756
PAO+2.5%[THTDP][Phos]	0.1267	4.3267
PAO+0.5%[THTDP][DCN]	0.1167	4.4156
PAO+1%[THTDP][DCN]	0.1089	4.6863
PAO+2.5%[THTDP][DCN]	0.0987	4.525

When the ILs were used as neat lubricants, Carreau's model could not be set up correctly as there was insufficient information regarding the viscosity of these fluids and this meant that either α^* could not be calculated, or the value was incorrect. The current laboratory setup also does not have the means to determine α^* experimentally. The comparison between the experimental results and the results for PAO and PAO mixtures with IL from Carreau's model are depicted in figures 19-21.

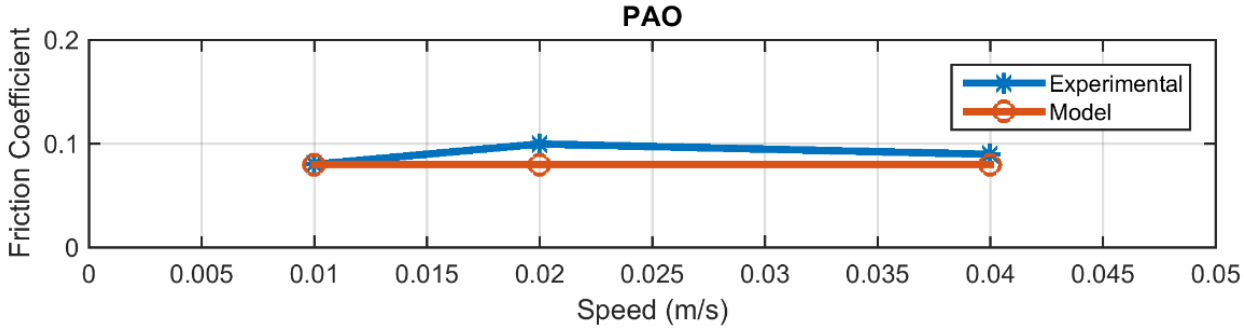

Figure 19: Comparison between experimental results and Carreau's Model for PAO (base oil)

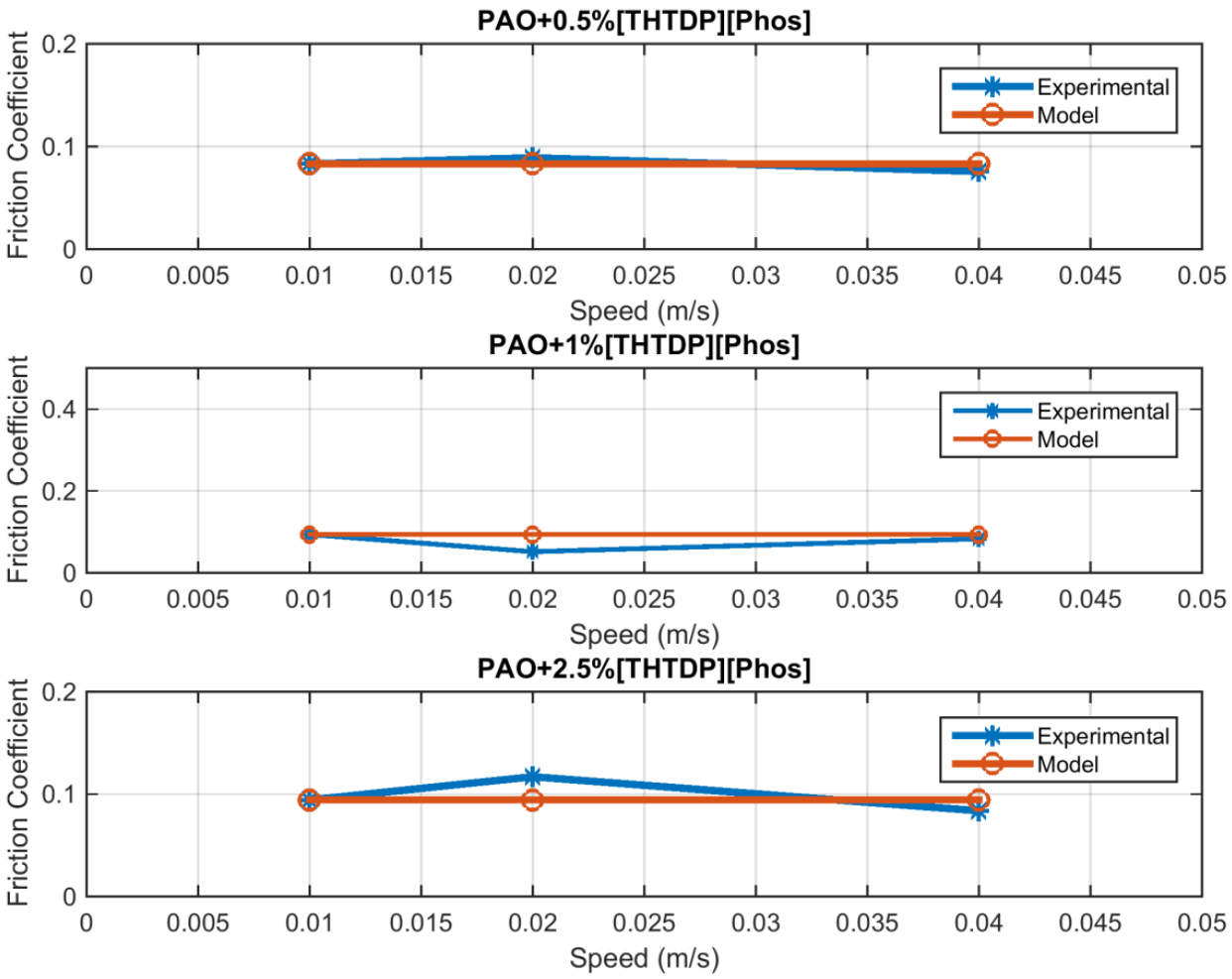

Figure 20: Comparison between experimental results and Carreau's Model using [THTDP][Phos] as an additive to PAO

From Figure 19, a good agreement between the theoretical and experimental results is observed when the PAO is used as a lubricant.

When [THTDP][Phos] is used as an additive, small deviation between the experimental and theoretical results is observed, confirming that the model is valid for use with these lubricants.

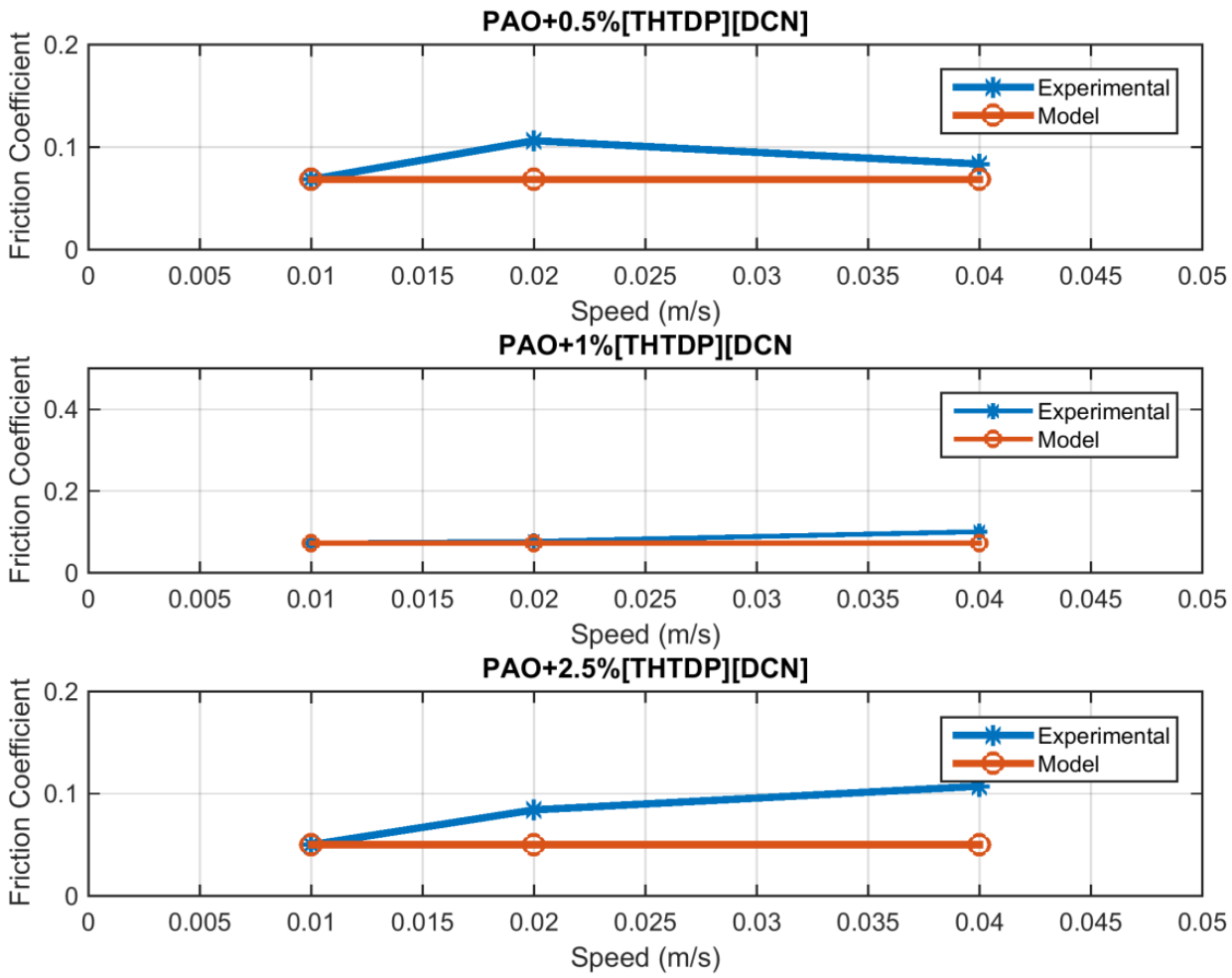

Figure 21: Comparison between experimental results and Carreau's Model using [THTDP][DCN] as an additive to PAO

The results with [THTDP][DCN] (Figure 21) are fairly good, but it is important to note that as the concentration of the IL is increased, there is a larger deviation from the theoretical value, at the highest value of speed studied. This deviation can be explained due to the formation of a corrosion resistant tribo-layer, which may have formed due to the increase in temperature at this speed. The formation of this layer can be verified by observing the wear results, which are discussed in the following section.

The root mean square error values between the theoretical and experimental results are depicted in Table 8.

Table 8: Root Mean Square (RMS) error values between the theoretical and experimental results for each lubricant

Lubricant	RMS Error
PAO	0.0110
PAO+0.5%[THTDP][Phos]	0.0048
PAO+1%[THTDP][Phos]	0.0217
PAO+2.5%[THTDP][Phos]	0.0125
PAO+0.5%[THTDP][DCN]	0.0203
PAO+1%[THTDP][DCN]	0.0141
PAO+2.5%[THTDP][DCN]	0.0333

The above table gives us a numerical estimate of the closeness of the fit between the theoretical and experimental results. We see that the deviation is small in the case of the PAO and when [THTDP][Phos] is added. A slightly larger deviation is observed when 2.5% of [THTDP][DCN] is added. This is in accordance with Figures 19-21.

6.4 Wear

The wear volume for each test was calculated using Eq. 14. The wear results at each speed are depicted in figures 22-27. As the surface roughness values at each speed are different, comparisons between lubricants can be made at the same speed only. The results at a speed of 0.01 m/s are depicted in Figure 22. At this speed, the addition of the ILs actually increases the amount of wear in the samples with [THTDP][DCN] performing better. This could be due to the fact that ILs require a certain amount of activation energy before they actually react with the surface and this speed, being fairly low, could not provide this required energy.

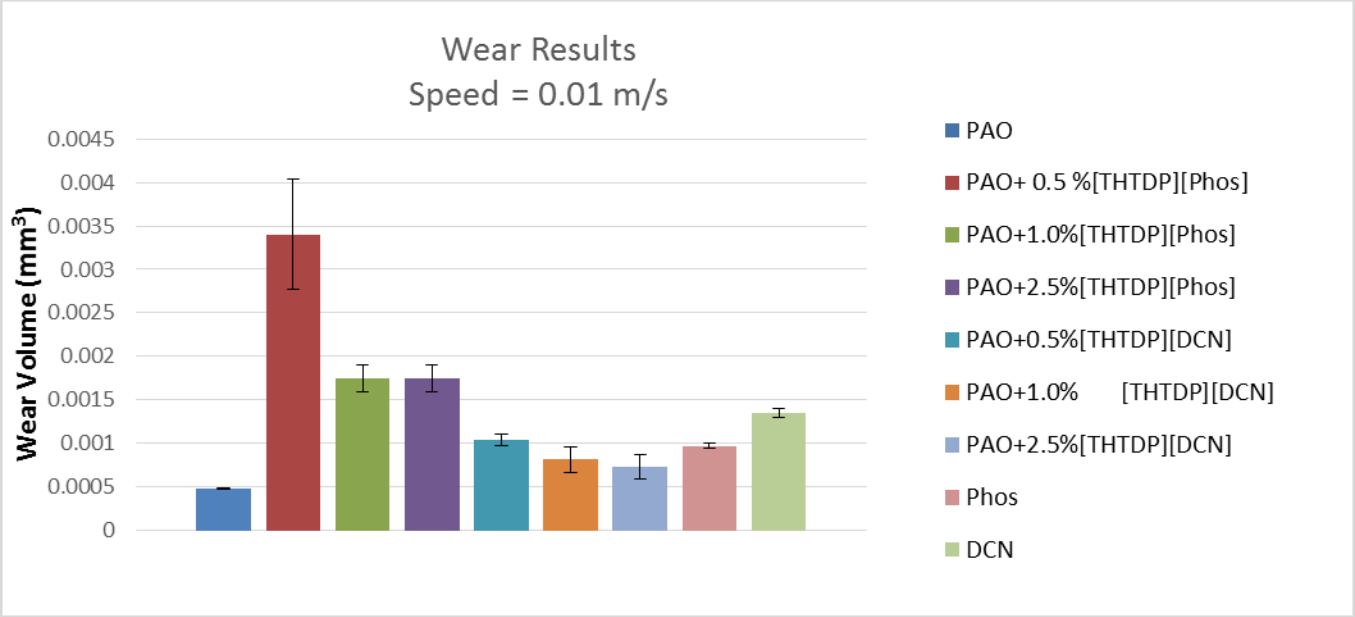

Figure 22: Summary of wear results at 0.01 m/s

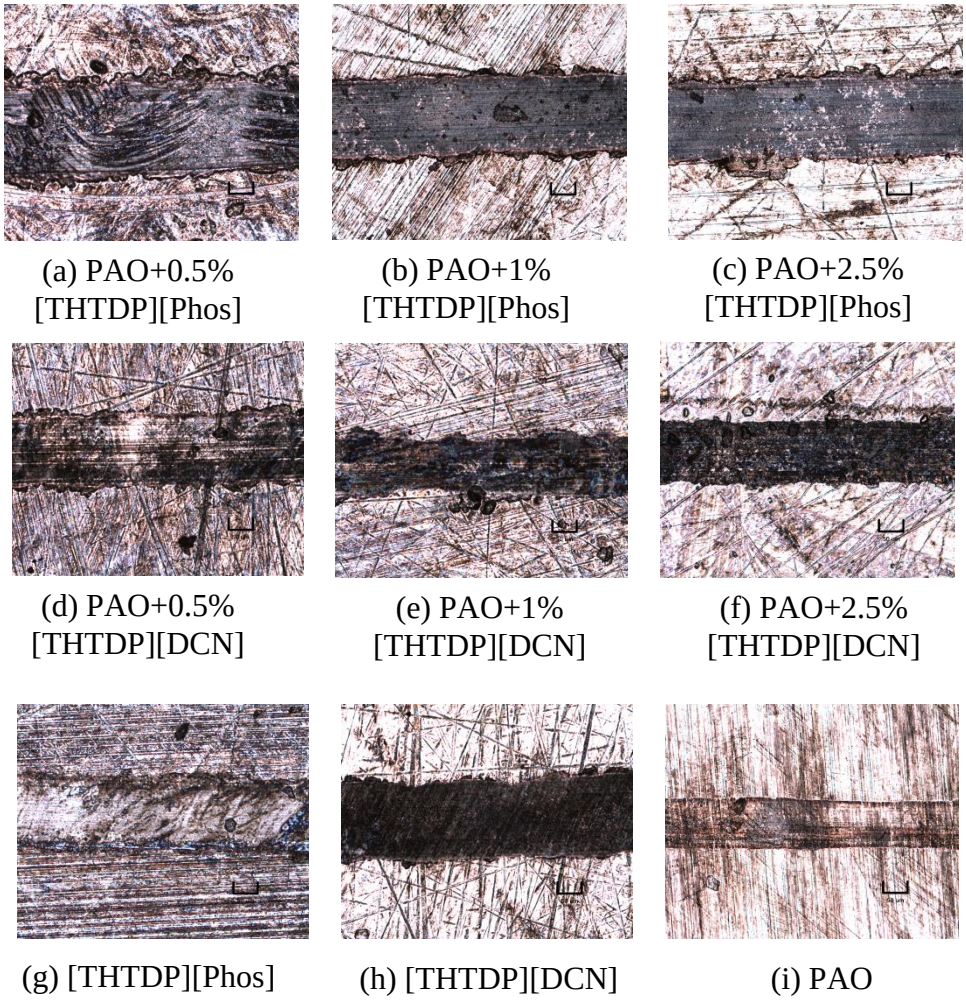

(a) PAO+0.5% [THTDP][Phos] (b) PAO+1% [THTDP][Phos] (c) PAO+2.5% [THTDP][Phos]

(d) PAO+0.5% [THTDP][DCN] (e) PAO+1% [THTDP][DCN] (f) PAO+2.5% [THTDP][DCN]

(g) [THTDP][Phos] (h) [THTDP][DCN] (i) PAO

Figure 23: Optical micrographs at 0.01 m/s

The optical micrographs of the samples tested at a speed of 0.01 m/s are shown in Figure 23. The addition of the ILs increase the amount of wear at this speed. Signs of abrasive wear (parallel lines and grooves in the wear track) and plastic deformation are visible when the ILs are used.

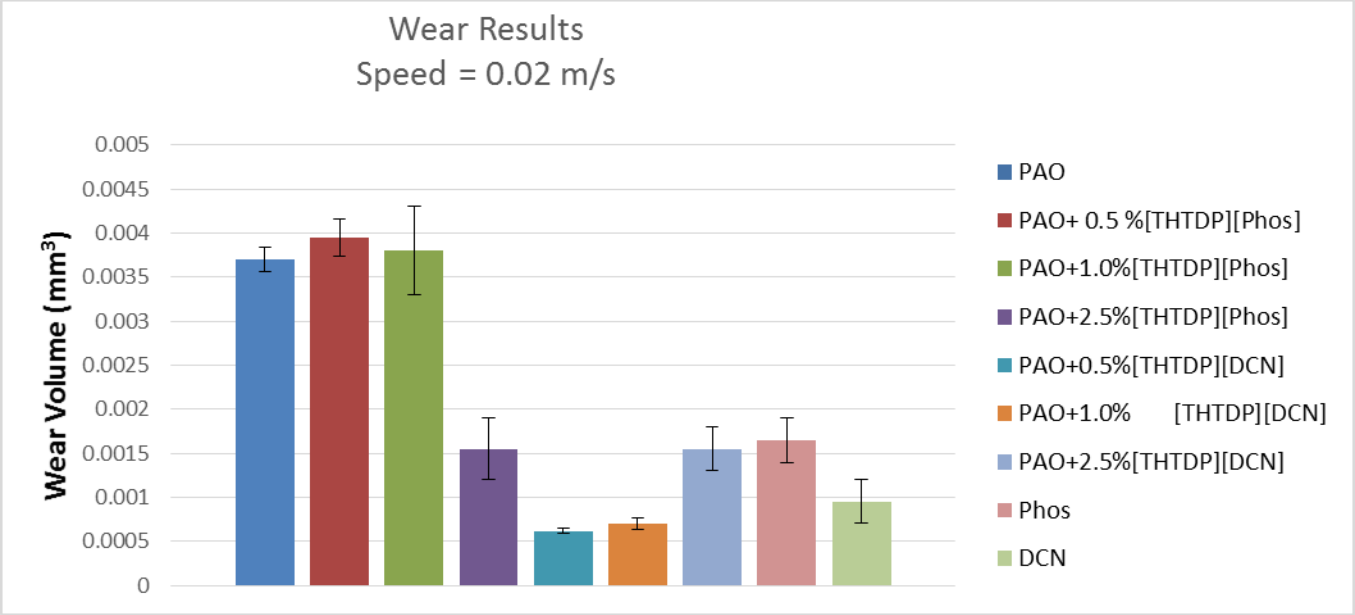

Figure 24: Summary of wear results at 0.02 m/s

Figure 24 shows the summary of the wear results at 0.04 m/s. From the figure, when 2.5% of [THTDP][Phos] and all concentrations of [THTDP][DCN] are used, a significant reduction in the wear volume is observed. There is an 83% decrease in the wear volume when 0.5% of [THTDP][DCN] is added when compared to the base oil and a 58% reduction when 2.5% of [THTDP][Phos] is added to the PAO. It should also be noted that there is a significant reduction in wear when the ILs are used as neat lubricants. The optical micrographs of the samples are presented in Figure 23.

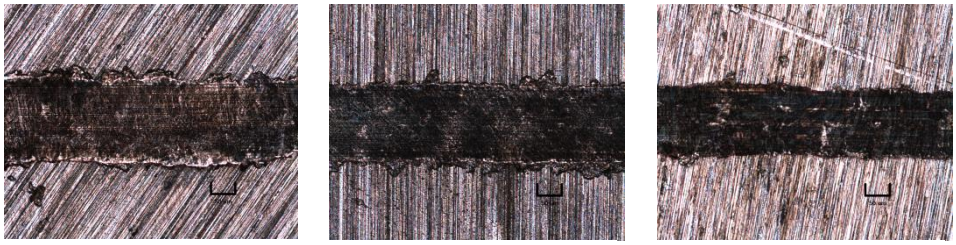

(a) PAO+0.5% [THTDP][Phos]

(b) PAO+1% [THTDP][Phos]

(c) PAO+2.5% [THTDP][Phos]

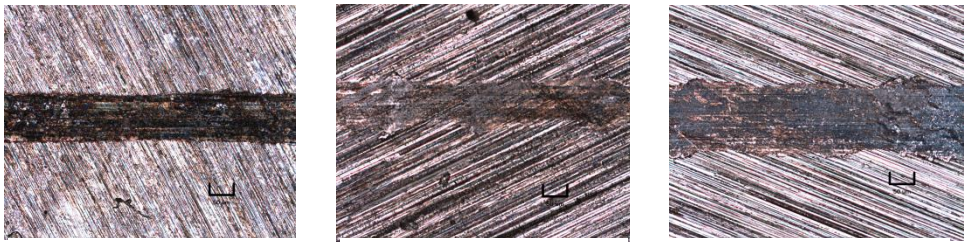

(d) PAO+0.5% [THTDP][DCN]

(e) PAO+1% [THTDP][DCN]

(f) PAO+2.5% [THTDP][DCN]

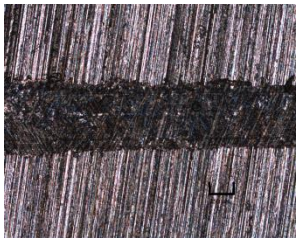

(g) [THTDP][Phos]

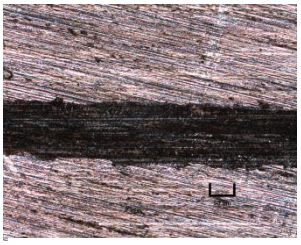

(h) [THTDP][DCN]

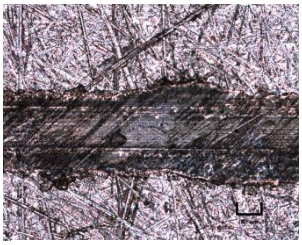

(i) PAO

Figure 25: Optical micrographs at 0.02 m/s

The wear scar of the base oil PAO shows abrasive wear but when the ILs are added, we don't see any abrasive wear. Also the amount of plastic deformation is clearly reduced when the ILs are added.

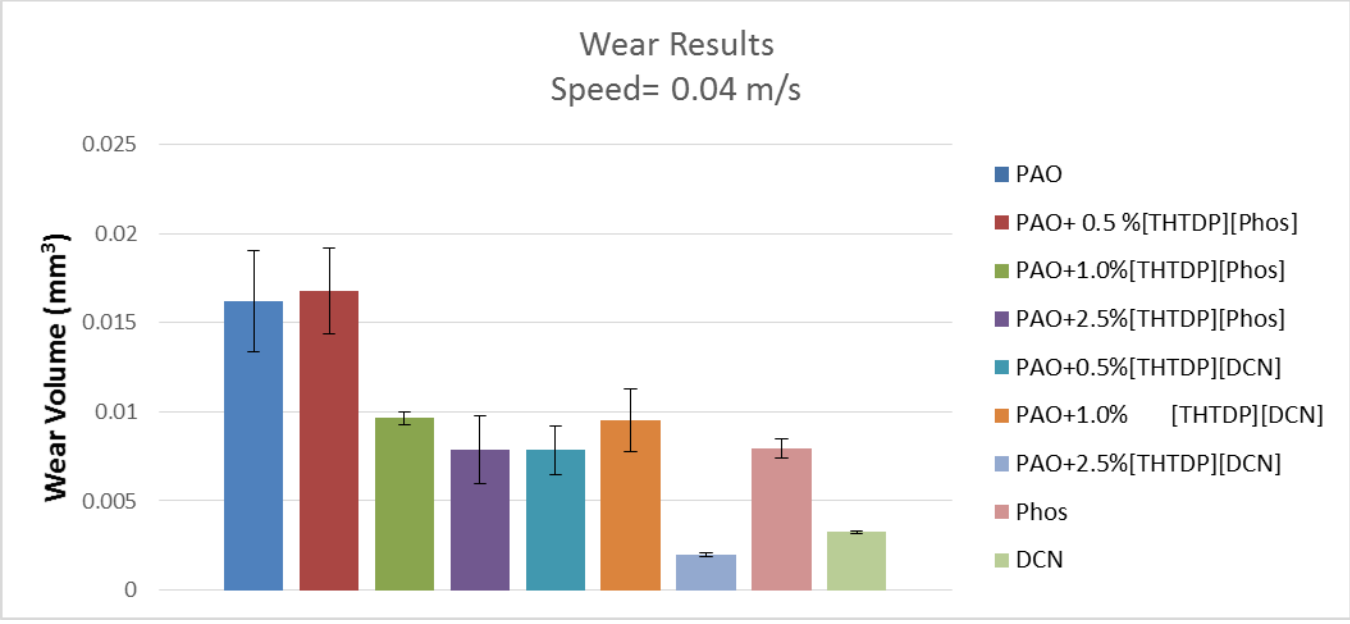

Figure 26: Summary of wear results at 0.04 m/s

At the highest speed of this study, both ILs perform very well except when 0.5% of [THTDP][Phos] is added. The most probable reason for this is that at this speed, the activation energy required for the reaction between the ILs and the metal surface is higher, thereby increasing the reactivity and facilitating the formation of a corrosion resistant tribolayer. As the concentration of [THTDP][Phos] is increased, the reduction in the wear volume increases. The greatest reduction (74%) is found when 2.5% of [THTDP][DCN] is used

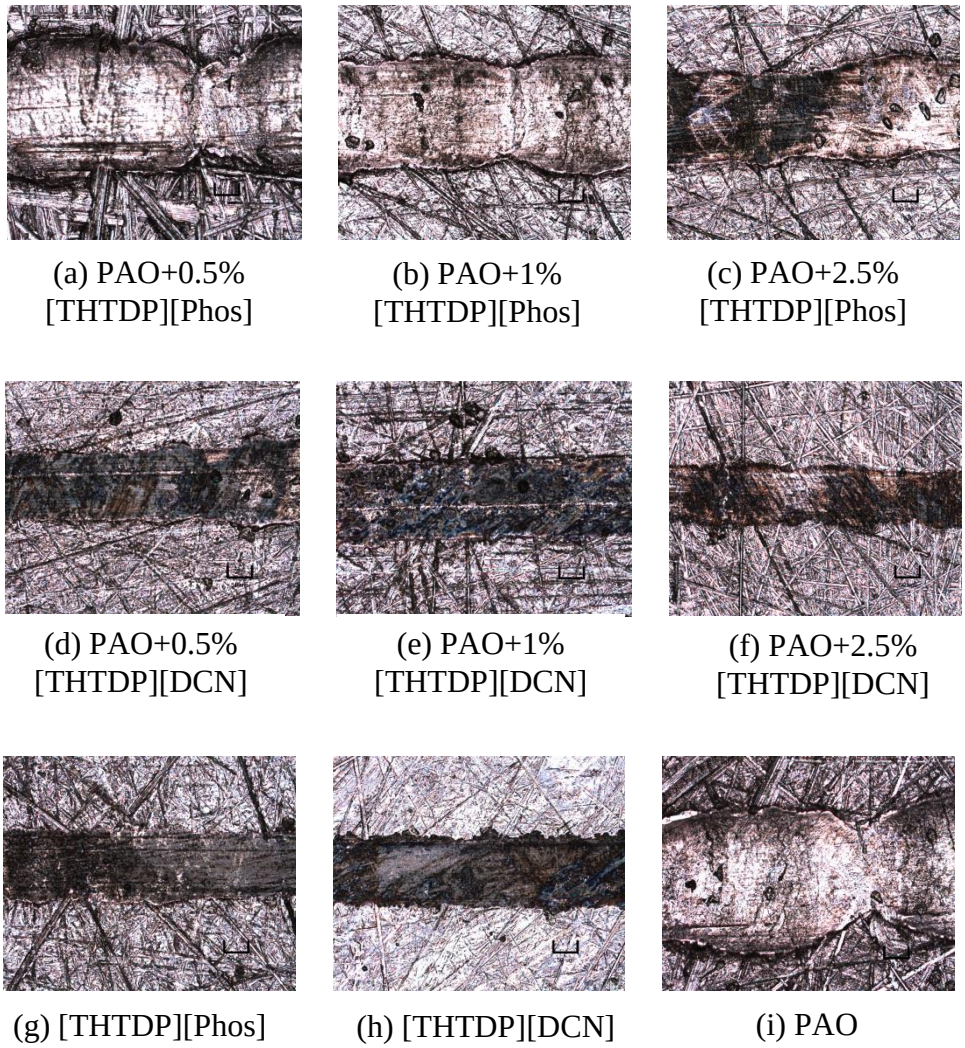

(a) PAO+0.5% [THTDP][Phos] (b) PAO+1% [THTDP][Phos] (c) PAO+2.5% [THTDP][Phos]

(d) PAO+0.5% [THTDP][DCN] (e) PAO+1% [THTDP][DCN] (f) PAO+2.5% [THTDP][DCN]

(g) [THTDP][Phos] (h) [THTDP][DCN] (i) PAO

Figure 27: Optical micrographs at 0.04 m/s

Figure 25 shows the optical micrographs of the samples. The test with the PAO indicates that the tracks are deeper and also the effect of vibrations in the machine are imparted on the track causing the widening and narrowing of the track at intervals. This phenomenon starts to vanish as the ILs are added and the best wear track is observed when 2.5% of [THTDP][DCN] is used. The neat ILs

also prove to be very good in reducing the amount of wear, as is evident from the optical micrographs.

7. CONCLUSIONS

In this study, the tribological behavior of two phosphonium-based ILs, Tetradecyltrihexylphosphonium bis(2,4,4-trimethylpentyl)phosphinate [THTDP][Phos] and Trihexyltetradecylphosphonium Decanoate [THTDP][DCN], is investigated as additives of a synthetic polyalphaolefin oil—Synton PAO-40 (PAO)—in steel–steel contact. PAO-IL blends containing between 0.5% wt. to 2.5% wt. of each IL are investigated using a block-on-flat reciprocating tribometer and the experimental results are compared to the results obtained from an existing elastohydrodynamic friction model. The following conclusions can be drawn from this study.

- Halogen-free Ionic Liquids can be used to decrease the friction and wear volume.
- There is not a large increase in the viscosity when the ILs are added to the PAO.
- [THTDP][Phos] is a non-Newtonian fluid and exhibits shear thinning behavior.
- [THTDP][DCN] is a Newtonian fluid.
- Carreau's model can be used to describe the behavior of [THTDP][Phos], when used as an additive to a base oil (PAO) for the concentrations and speeds used in this study.
- Carreau's model can describe the behavior of [THTDP][DCN] when used as an additive to the base oil at slower speeds. It is less accurate at higher speeds due to the increase in activation energy, thereby resulting in the formation of a tribolayer.
- At a speed of 0.02m/s, a 58% reduction in wear volume is found when 2.5% [THTDP][Phos] is added to the PAO and an 83% reduction in wear volume is observed when 0.5% of [THTDP][DCN] is added to the base oil.
- At 0.04 m/s, a mixture of PAO and 2.5% [THTDP][DCN] reduces the wear volume by 74% when compared to the base oil.
- The primary wear mechanisms observed are abrasive wear and plastic deformation. These effects are reduced considerably by the addition of the ILs.

8. SCOPE FOR FUTURE WORK

- Experimental determination of the pressure-viscosity coefficient will mostly provide more accurate results. Also will enable the prediction of the friction coefficient using these specific neat ionic liquids.
- Studying different models, and comparing their results to Carreau's model, thereby identifying the best model.
- Combining the results from all such models and from using different ionic liquids could facilitate the creation of a theoretical model solely for ionic liquids.

9. REFERENCES

[1] Holmberg, K., Andersson, P., and Erdemir, A., 2012, "Global energy consumption due to friction in passenger cars," Tribol. Int., **47**, pp. 221–234.

[2] Tzanakis, I., Hadfield, M., Thomas, B., Noya, S. M., Henshaw, I., and Austen, S., 2012, "Future perspectives on sustainable tribology," Renew. Sustain. Energy Rev., **16**(6), pp. 4126–4140.

[3] Ye, C., Liu, W., Chen, Y., and Yu, L., 2001, "Room-temperature ionic liquids: a novel versatile lubricant.," Chem. Commun. (Camb)., (21), pp. 2244–2245.

[4] Zhou, F., Liang, Y., and Liu, W., 2009, "Ionic liquid lubricants: designed chemistry for engineering applications.," Chem. Soc. Rev., **38**(9), pp. 2590–2599.

[5] Kondo, Y., Koyama, T., and Sasaki, S., 2013, "Tribological Properties of Ionic Liquids," Ion. Liq. - New Asp. Futur.

[6] Song, Z., Liang, Y., Fan, M., Zhou, F., and Liu, W., 2014, "Ionic liquids from amino acids: fully green fluid lubricants for various surface contacts," RSC Adv., **4**(37), pp. 19396–19402.

[7] Jiménez, a. E., Bermúdez, M. D., Iglesias, P., Carrión, F. J., and Martínez-Nicolás, G., 2006, "1-N-alkyl -3-methylimidazolium ionic liquids as neat lubricants and lubricant additives in steel-aluminium contacts," Wear, **260**(7-8), pp. 766–782.

[8] Jiménez, A. E., and Bermúdez, M. D., 2009, "Ionic liquids as lubricants of titanium-steel contact," Tribol. Lett., **33**(2), pp. 111–126.

[9] Bermúdez, M. D., Jiménez, A. E., Sanes, J., and Carrión, F. J., 2009, "Ionic liquids as advanced lubricant fluids," Molecules, **14**(8), pp. 2888–2908.

[10] Fajardo, O. Y., Bresme, F., Kornyshev, a. a., and Urbakh, M., 2015, "Electrotunable Lubricity with Ionic Liquid Nanoscale Films," Sci. Rep., **5**, p. 7698.

[11] Jacod, B., 2002, "Friction in elasto-hydrodynamic lubrication," University of Twente.

[12] 2015, "Stachowiak, Gwidon, and Batchelor, A. W.. Engineering Tribology (3rd Edition). Burlington, MA, USA: Butterworth-Heinemann, 2005. ProQuest ebrary. Web. 2 June 2015. Copyright © 2005. Butterworth-Heinemann. All rights reserved."

[13] Hooke, C., 2009, "A review of the paper 'A numerical solution to the elastohydrodynamic problem' by D. Dowson and G. R. Higginson," Proc. Inst. Mech. Eng. Part C J. Mech. Eng. Sci., **223**(1), pp. 49–63.

[14] Barus, C., 1893, "Isothermals, isopiestics and isometrics relative to viscosity."

[15] Roelands, C., 1966, “Correlational Aspects of the Viscosity-Temperature Pressure Relationship of Lubricating Oils,” (April), p. 495.

[16] Spikes, H., and Jie, Z., 2014, “History, Origins and Prediction of Elastohydrodynamic Friction,” Tribol. Lett., **56**(1), pp. 1–25.

[17] Otero, J. E., Morgado, P. L., Sánchez-Peñuela, J. B., Sanz, J. L. M., Munoz-Guijosa, J. M., Lantada, A. D., and Yustos, H. L., 2009, “Elastohydrodynamic Models for Predicting Friction in Point Contacts Lubricated with Polyalphaolefins,” Proceedings of EUCOMES 08 SE - 27, M. Ceccarelli, ed., Springer Netherlands, pp. 219–227.

[18] NISHIKAWA, H., HANDA, K., and KANETA, M., 1992, “Behavior of EHL Films in Reciprocating Motion.,” Trans. Japan Soc. Mech. Eng. Ser. C, **58**(550), pp. 1911–1918.

[19] Morgado, P. L., Otero, J. E., Lejarraga, J. B. S.-P., Sanz, J. L. M., Lantada, a D., Munoz-Guijosa, J. M., Yustos, H. L., Wiña, P. L., and García, J. M., 2009, “Models for predicting friction coefficient and parameters with influence in elastohydrodynamic lubrication,” Proc. Inst. Mech. Eng. Part J J. Eng. Tribol., **223**(7), pp. 949–958.

[20] Minami, I., 2009, “Ionic liquids in tribology.,” Molecules, **14**(6), pp. 2286–2305.

[21] Xiao, H., Guo, D., Liu, S., Pan, G., and Lu, X., 2011, “Film thickness of ionic liquids under high contact pressures as a function of alkyl chain length,” Tribol. Lett., **41**(2), pp. 471–477.

[22] Pensado, a. S., Comuñas, M. J. P., and Fernández, J., 2008, “The pressure-viscosity coefficient of several ionic liquids,” Tribol. Lett., **31**(2), pp. 107–118.

[23] Totolin, V., Minami, I., Gabler, C., and Dörr, N., 2013, “Halogen-free borate ionic liquids as novel lubricants for tribological applications,” Tribol. Int., **67**, pp. 191–198.

[24] Gusain, R., Singh, R., Sivakumar, K. L. N., and Khatri, O. P., 2014, “Halogen-free imidazolium/ammonium-bis(salicylato)borate ionic liquids as high performance lubricant additives,” RSC Adv., **4**(3), p. 1293.

[25] Minami, I., Inada, T., Sasaki, R., and Nanao, H., 2010, “Tribo-chemistry of phosphonium-derived ionic liquids,” Tribol. Lett., **40**(2), pp. 225–235.

[26] Harris, K. R., Woolf, L. a, and Kanakubo, M., 2005, “Temperature and Pressure Dependence of the Viscosity of the Ionic Liquid 1-Butyl-3-methylimidazolium Hexafluorophosphate,” J. Chem. Eng. Data, **50**(5), pp. 1777–1782.

[27] Harris, L. K. R., Kanakubo, M., Woolf, a, and Data, J. C. E., 2008, “Temperature and Pressure Dependence of the Viscosity of the Ionic Liquid 1-Butyl-3-methylimidazolium Tetrafluo- roborate : Viscosity and Density Relationships in Ionic,” **2**(1), p. 800181.

[28] Harris, K. R., Kanakubo, M., and Woolf, L. a., 2007, "Temperature and pressure dependence of the viscosity of the ionic liquids 1-hexyl-3-methylimidazolium hexafluorophosphate and 1-butyl-3-methylimidazolium BiS(trifluoromethylsulfonyl)imide," J. Chem. Eng. Data, **52**(3), pp. 1080–1085.

[29] Tomida, D., Kumagai, a., Qiao, K., and Yokoyama, C., 2006, "Viscosity of [bmim][PF6] and [bmim][BF4] at high pressure," Int. J. Thermophys., **27**(1), pp. 39–47.

[30] Tomida, D., Kumagai, A., Kenmochi, S., Qiao, K., and Yokoyama, C., 2007, "Viscosity of 1-hexyl-3-methylimidazolium hexafluorophosphate and 1-octyl-3-methylimidazolium hexafluorophosphate at high pressure," J. Chem. Eng. Data, **52**(2), pp. 577–579.

[31] Kandil, M. E., Marsh, K. N., and Goodwin, A. R. H., 2007, "Measurement of the viscosity, density, and electrical conductivity of 1-hexyl-3-methylimidazolium bis(trifluorosulfonyl)imide at temperatures between (288 and 433) K and pressures below 50 MPa," J. Chem. Eng. Data, **52**(6), pp. 2382–2387.

[32] Bair, S., Liu, Y., and Wang, Q. J., 2006, "The Pressure-Viscosity Coefficient for Newtonian EHL Film Thickness With General Piezoviscous Response," J. Tribol., **128**(3), p. 624.

[33] Fein, R., 1997, "High Pressure Viscosity and EHL Pressure-Viscosity Coefficients," Tribology Data Handbook, CRC Press.

[34] Leeuwen, H. Van, 2009, "The determination of the pressure–viscosity coefficient of a lubricant through an accurate film thickness formula and accurate film thickness measurements," Proc. Inst. Mech. Eng. Part J J. Eng. Tribol., **223**(8), pp. 1143–1163.

[35] Moes, H., 2000, "Lubrication and beyond," Utwente Lect. notes, p. 366.

[36] Qu, J., and Truhan, J. J., 2006, "An efficient method for accurately determining wear volumes of sliders with non-flat wear scars and compound curvatures," Wear, **261**(7-8), pp. 848–855.

[37] Bair, S., Vergne, P., and Querry, M., 2005, "A unified shear-thinning treatment of both film thickness and traction in EHD," Tribol. Lett., **18**(2), pp. 145–152.

10. APPENDICES

Appendix A: MATLAB Code to estimate Pressure-Viscosity Coefficent

```
clc
v40=3310;                              %Viscosity at 40 C (Change for each Lubricant)
v100=2180;                             %Viscosity at 100 C (Change for each Lubricant)
H40=log10(log10(v40)+1.200);           %H40
H100=log10(log10(v100)+1.200);         %H100
a=H40-H100;
F40=(0.885-0.864*H40);                 %F40
v0=3310/1000;                          %Viscosity at Temperature at which alpha is desired
z=((7.81*a)^1.5)*F40                   %Calculation of z
pr=1.98*10^8;
vinf=6.315*10^-5;
a1=log(v0/vinf)*z/pr                   %Calculation of Barus Pressure Viscosity Coefficient
astar=a1/(1+((1-z)/(a1*pr)))           %Calculation of Bloks Isoviscosu Pressure Coefficient
```

Appendix B: MATLAB Code to calculate central film thickness, contact pressure and film parameter.

```
v0=3310/1000;                              %Viscosity at 40 C (Change for each Lubricant)
U=0.005/2;                                 %Average sliding speed
E1=210e9;                                  %Youngs modulus of Steel Sample
E2=200e9;                                  %Youngs modulus of Steel Ball
v1=0.3;                                    %Poissons Ratio of Steel Sample
v2=0.27;                                   %Poissons Ratio of Steel Ball
E_1=(((1-v1^2)/E1)+((1-v2^2)/E2));
E=1/E_1;                                   %Equivalent Youngs Modulus
R=(2/(1.5*10^-3))^-1;                      %Reduced radius of curvature
a=7.1938e-11;                              %Pressure-Viscosity Coefficient
W=5;                                       %Load(N)
h=1.39*((v0*U/(2*E*R)^0.67)*((a*E)^0.53)*((E*R*R/W)^0.067));  %Film Thickness
s2=0.05e-6;                                %Roughness of Steel Ball
s1=sqrt((h^2/9)-s2^2);                     %Estimate roughness of Steel Smaple
s11=sqrt((h^2/100)-s2^2);
s1=0.4e-6;
l=h/sqrt(s1^2+s2^2);                      %Film Parameter
a1=(3*W*R/(4*E))^(1/3);                   %Area of contact
p=3*W/(2*pi*a1^2);                        %Contact Pressure
```

Appendix C: MATLAB Code to calculate the friction coefficient and compare with experimental results.

```
%Carreau's Model for [THTDP][Phos]
clc
Film
dU=[0.005,0.01,0.02]*2;                     % Sliding Speed of Voice Coil
U=dU/2;                                     % Average sliding speed of both surfaces
n=[0.1235,0.1242,0.1275,0.1267];            % Values of 'n' in Carreaus Model for each Lubricant
G=[4.2859,4.3415,4.2756,4.3267]*10^6;       % Values of 'G' in Carreaus Model for each Lubricant
v0=[325,330.09,330.35,331.99]/1000;         % Viscosity of each lubricant
a=[16.379,16.389,16.474,16.553]*10^-9;      % Pressure-Viscosity Coefficient
cm=zeros(4,3);
h=0;
for i=1:4;
    for j=1:3;
h=1.39*((v0(i)*U(j)/(2*E*R)^0.67)*((a(i)*E)^0.53)*((E*R*R/W)^0.067));     % Calculation of Film
Thickness
cm(i,j)=3*((v0(i).*dU(j)/h).^n(i))*(G(i).^(1-n(i)))*(exp(n(i).*a(i)*p)*(n(i).*a(i)*p-
1)+1)/((n(i).*a(i)).^2*p.^3);               % Calculation of Friction Coefficient
    end
end
cex=[0.080123,0.099823,0.089858;0.08306,0.089,0.075628;0.093643,0.051566,0.083057;0.094253,0.1169
58,0.083684];                               % Experimental friction values for each lubricant
figure
subplot(3,1,1)
plot(dU,cex(1,:),'-*',...
    'LineWidth',2)
hold on
plot(dU,cm(1,:),'-o',...
    'LineWidth',2)
legend('Experimental','Model')
title('PAO')
xlabel('Speed (m/s)')
ylabel('Friction Coefficient')
axis([0,0.05,0,0.5])
grid on
hold off
subplot(3,1,1)
plot(dU,cex(2,:),'-*',...
    'LineWidth',2)
hold on
plot(dU,cm(2,:),'-o',...
    'LineWidth',2)
 legend('Experimental','Model')
title('PAO+0.5%[THTDP][Phos]')
xlabel('Speed (m/s)')
ylabel('Friction Coefficient')
axis([0,0.05,0,0.5])
grid on
hold off
subplot(3,1,2)
```

```
plot(dU,cex(3,:),'-*',...
    'LineWidth',2)
hold on
plot(dU,cm(3,:),'-o',...
    'LineWidth',2)
 legend('Experimental','Model')
title('PAO+1%[THTDP][Phos]')
ylabel('Friction Coefficient')
xlabel('Speed (m/s)')
axis([0,0.05,0,0.5])
grid on
subplot(3,1,3)
plot(dU,cex(4,:),'-*',...
    'LineWidth',2)
hold on
plot(dU,cm(4,:),'-o',...
    'LineWidth',2)
 legend('Experimental','Model')
title('PAO+2.5%[THTDP][Phos]')
xlabel('Speed (m/s)')
ylabel('Friction Coefficient')
axis([0,0.05,0,0.5])
grid on
hold off
for i=1:4;
rms1p(i)=sqrt(sum((cm(i,:)-cex(i,:)).^2)/length(cm));                                    %
Calculation of RMS error values
end
```

```
%Carreau's Model for [THTDP][DCN]
clc
Film
dU=[0.005,0.01,0.02]*2;                    % Sliding Speed of Voice Coil
U=dU/2;                                    % Average sliding speed of both surfaces
n=[0.1235,0.1167,0.1089,0.0987];           % Values of 'n' in Carreaus Model for each Lubricant
G=[4.2859,4.4156,4.6863,4.525]*10^6;       % Values of 'G' in Carreaus Model for each Lubricant
v0=[325,339,360,343.3]/1000;               % Viscosity of each lubricant
a=[16.379,16.514,17.52,17.563]*10^-9;      % Pressure-Viscosity Coefficient
cm=zeros(4,3);

for i=1:4;
    for j=1:3;
h=1.39*((v0(i)*U(j)/(2*E*R)^0.67)*((a(i)*E)^0.53)*((E*R*R/W)^0.067));  % Calculation of Film
Thickness
cm(i,j)=3*((v0(i).*dU(j)/h).^n(i))*(G(i).^(1-n(i)))*(exp(n(i).*a(i)*p)*(n(i).*a(i)*p-
1)+1)/((n(i).*a(i)).^2*p.^3);              % Calculation of Friction Coefficient
    end
end
cex=[0.080123,0.099823,0.089858;0.068537,0.10628,0.083547;0.07274,0.076889,0.10048;0.050008,0.084
181,0.107319];    % Experimental friction values for each lubricant
figure
subplot(2,2,1)
plot(dU,cex(1,:),'-*',...
    'LineWidth',2)
```

```
hold on
plot(dU,cm(1,:),'-o',...
    'LineWidth',2)
legend('Experimental','Model')
title('Model vs Experiment PAO')
ylabel('Friction Coefficient')
xlabel('Speed (m/s)')
axis([0,0.05,0,0.5])
grid on
subplot(2,2,2)
plot(dU,cex(2,:),'-*',...
    'LineWidth',2)
hold on
plot(dU,cm(2,:),'-o',...
    'LineWidth',2)
legend('Experimental','Model')
title('PAO+0.5%[THTDP][DCN]')
ylabel('Friction Coefficient')
xlabel('Speed (m/s)')
axis([0,0.05,0,0.5])
grid on
subplot(2,2,3)
plot(dU,cex(3,:),'-*',...
    'LineWidth',2)
hold on
plot(dU,cm(3,:),'-o',...
    'LineWidth',2)
legend('Experimental','Model')
title('PAO+1%[THTDP][DCN')
ylabel('Friction Coefficient')
xlabel('Speed (m/s)')
axis([0,0.05,0,0.5])
grid on
subplot(2,3,4)
plot(dU,cex(4,:),'-*',...
    'LineWidth',2)
hold on
plot(dU,cm(4,:),'-o',...
    'LineWidth',2)
legend('Experimental','Model')
title('PAO+2.5%[THTDP][DCN]')
ylabel('Friction Coefficient')
xlabel('Speed (m/s)')
axis([0,0.05,0,0.5])
grid on
for i=1:4;
rms1(i)=sqrt(sum((cm(i,:)-cex(i,:)).^2)/length(cm));            % Calculation of RMS error values
end
```